TU Delft

Delft University of Technology

A solid oxide fuel cell- supercritical carbon dioxide Brayton cycle hybrid system

Schöffer, S. I.; Klein, S. A.; Aravind, P.V.; Pecnik, R.

DOI
10.1016/j.apenergy.2020.115748

Publication date
2021

Document Version
Final published version

Published in
Applied Energy

Citation (APA)
Schöffer, S. I., Klein, S. A., Aravind, P. V., & Pecnik, R. (2021). A solid oxide fuel cell- supercritical carbon dioxide Brayton cycle hybrid system. *Applied Energy*, *283*, Article 115748. https://doi.org/10.1016/j.apenergy.2020.115748

Important note
To cite this publication, please use the final published version (if applicable).
Please check the document version above.

Copyright
Other than for strictly personal use, it is not permitted to download, forward or distribute the text or part of it, without the consent of the author(s) and/or copyright holder(s), unless the work is under an open content license such as Creative Commons.

Takedown policy
Please contact us and provide details if you believe this document breaches copyrights.
We will remove access to the work immediately and investigate your claim.

This work is downloaded from Delft University of Technology.
For technical reasons the number of authors shown on this cover page is limited to a maximum of 10.

Applied Energy 283 (2021) 115748

Contents lists available at ScienceDirect

Applied Energy

journal homepage: www.elsevier.com/locate/apenergy

A solid oxide fuel cell- supercritical carbon dioxide Brayton cycle hybrid system

S.I. Schöffer *, S.A. Klein, P.V. Aravind, R. Pecnik

Department of Process&Energy, Delft University of Technology, Netherlands

A B S T R A C T

New technologies are being developed to produce electricity cleaner and more efficient. Promising technologies among these are the solid oxide fuel cell and the supercritical carbon dioxide Brayton cycle. This study investigates the potential of integrating both technologies.

The solid oxide fuel cell is known as a potentially clean and highly efficient technology to convert chemical energy to electricity. The high operating temperatures (600–1000 °C) allow the possibility of a bottoming cycle to utilize the high quality excess heat and also facilitate reforming processes, making it possible to use higher hydrocarbons as fuel.

The supercritical carbon dioxide Brayton cycle has received attention as a promising power cycle. It has already been identified as a suitable cycle for relatively low temperature, compared to traditional gas turbines, heat sources for several reasons.

Firstly because of the high efficiency, around 40%–45% for the common simple recuperative cycle. Secondly, because the turbine inlet temperature of a supercritical carbon dioxide is around 700 °C is low, compared to well over 1000 °C for a common air Brayton cycle. This is especially of interest because solid oxide fuel cell developers are targeting lower operating temperatures to avoid the use of exotic and expensive materials. And thirdly, the cycle can operate entirely above the critical point. Therefore the temperature increases gradually with the energy added to the cycle. This is more suitable for waste heat because the exergy loss decreases and more low temperature heat can be utilized compared to a steam Rankine cycle where most of the heat is added above the relatively high boiling point of pressurized water.

A thermodynamic model of the solid oxide fuel cell- supercritical carbon dioxide Brayton cycle hybrid system is developed to explore and analyze different concepts of integration.

Several conclusions are drawn. Firstly it is found that recirculating cathodic air increases the efficiency of the system and decreases the size of the heat exchangers. Secondly, applying a pinch point optimization decreases the size of the heat exchangers but increases the complexity of the system while the efficiency is not much affected. Thirdly, applying the recompression cycle in stead of a simple recuperative supercritical carbon dioxide cycle increases the efficiency of the system but not as significantly when operating the supercritical carbon dioxide as a stand-alone system while the complexity of the system increases even more. And finally, compared to a directly coupled solid oxide fuel cell-gas turbine system the solid oxide fuel cell- supercritical carbon dioxide Brayton cycle hybrid system is more efficient but significantly more complex.

1. Introduction

On December 12, 2015, the United Nations Framework Convention on Climate Change reached an agreement to mitigate climate change. Key in reaching this goal is a cleaner and more efficient way of producing power. Traditional ways of power production will be phased out and replaced by renewable energy sources and cleaner fuel conversion systems.

The goal of this paper is to present the results and analysis of several case studies of a solid oxide fuel cell- supercritical carbon dioxide Brayton cycle hybrid system (SSHS).

Among other technologies, the solid oxide fuel cell (SOFC) has received attention as a potentially clean and highly efficient method of converting chemical energy to electricity. The high operating temperatures (600-1000 °C) allow the possibility of a bottoming cycle to utilize the high quality excess heat and also facilitate reforming processes, making it possible to use higher hydrocarbons as fuel [1].

Utilizing the waste heat of a SOFC system in a thermodynamic cycle is a well known concept. Fig. 1 illustrates the general concept. Fuel is consumed in a SOFC, producing electricity and heat. This heat is then transferred to a power cycle where part of it is converted to electricity and the remaining heat is rejected to the environment.

The sCO_2 Brayton cycle has received attention as a promising power cycle. It has already been identified as a suitable cycle for heat sources such as nuclear [2], exhaust/waste heat [3,4], geothermal [5] and concentrated solar power (CSP) [6,7].

These heat sources supply heat to a power cycle at lower temperatures than heat produced by combustion. The sCO_2 Brayton cycle is suitable for such a heat source for several reasons. Firstly because of the

* Corresponding author.
E-mail address: samuelschoffer@gmail.com (S.I. Schöffer).

https://doi.org/10.1016/j.apenergy.2020.115748
Received 9 March 2020; Received in revised form 7 August 2020; Accepted 18 August 2020
Available online 16 September 2020
0306-2619/© 2020 The Authors. Published by Elsevier Ltd. This is an open access article under the CC BY license (http://creativecommons.org/licenses/by/4.0/).

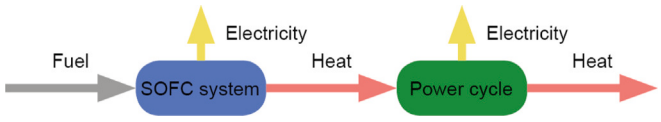

Fig. 1. General concept of a SOFC- bottoming cycle hybrid system.

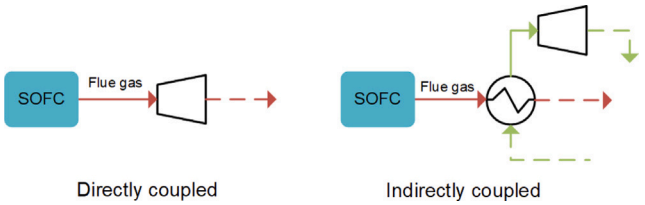

Fig. 2. Schematic view of a directly and indirectly coupled hybrid system.

high efficiency, around 40%–45% for the common simple recuperative cycle. Secondly, because the temperature range over which heat is added to the cycle is low compared to a common air Brayton cycle. The turbine inlet temperature (TIT) of a sCO_2 is around 700 °C compared to well over 1000 °C for a common air Brayton cycle. And thirdly, the cycle can operate entirely above the critical point. Therefore the temperature increases gradually with the energy added to the cycle. This is more suitable for waste heat because the exergy loss decreases and more low temperature heat can be utilized.

The sCO_2 therefore combines the advantages of the steam Rankine cycle, low compression work, and the air Brayton cycle, no phase change, but does not need a high TIT to achieve high efficiencies. The latter is especially of interest because SOFC developers are targeting lower operating temperatures to avoid the use exotic and expensive materials. Furthermore, the high density of the sCO_2 also makes for small and relatively simple turbomachinery [8].

Furthermore, carbon dioxide is abundantly available, cheap, stable and non-toxic [2].

Different concepts of a SOFC- bottoming cycle hybrid system exist and can be categorized based on several characteristics of the system.

Firstly, it is common to have a reformer as part of a SOFC system. In a reformer, fuel such as methane, reacts with water to syngas. The endothermic reforming process is driven by excess heat generated in the fuel cell. Three methods for transferring the heat from the fuel cell to the reformer are distinguished in general: Indirect internal reforming (IIR), direct internal reforming (DIR) and external reforming (ER). In case of IIR, the reformer is only thermally coupled to the fuel cell. The catalyst required for the reforming process can also be integrated into the anode. In such a setup, DIR, both the reforming- and electrochemical reactions take place in the anode. Having a separate reformer is an option as well, this is referred to as ER. The required steam for the reforming process can either be supplied by recirculating the outlet of anode, which contains steam, or externally by a heat recovery steam generator (HRSG).

Secondly, a bottoming cycle can either be directly coupled to the SOFC system or indirectly. In a directly coupled system, the exhaust gas of the SOFC system is integrated in a recuperated gas turbine to replace the combustor. In the GT the remaining fuel is combusted and the flue gas is expanded through the turbine to produce power. For this reason, the SOFC system is pressurized in a directly coupled setup. In an indirectly coupled system, such as the SSHS, the working fluids of SOFC system and the bottoming cycle are separated and the excess heat of the SOFC system is transferred to the bottoming cycle in heat exchangers (see Fig. 2).

Table 1 gives a summary of selected studies reviewed by Buonomano et al. [9] categorized by reforming method and thermal coupling of the power cycle. All systems use methane as fuel. It shows that high efficiencies of well over 60% are possible. Since not all studies have the same parameters such as the TIT and pressure ratio (PR), as well as different approaches to modeling and underlying assumptions it is hard to draw conclusions. However, some general remarks can be made.

It can be said that directly coupled hybrid systems have higher efficiencies and are less complex than indirectly coupled systems. Hence most research focuses on this type. Control strategies however prove to be difficult, making these systems unattractive for part-load operation. Conversely, indirectly coupled systems are more complex and less efficient but are more flexible in operation.

Finally it shows that having a more directly thermally coupled reforming system, DIR over IIR over ER, leads to higher efficiencies.

A sCO_2 Brayton cycle in combination with another high temperature fuel cell, a molten carbonate fuel cell (MCFC), has been studied. Bae et al. [19] conclude that the sCO_2 cycle is a more efficient bottoming cycle for the MCFC than an air Brayton cycle cycle. Various cycle layouts have been studied as a bottoming cycle for a MCFC system. The heat available from the MCFC is considered as a design constraint that is not varied. Consequently, integration concepts of the two systems and variation in the MCFC's operation and its effect on the sCO_2 Brayton cycle are not studied.

Integration of a SOFC system and a sCO_2 Brayton cycle has, to the authors knowledge, not been studied yet. This is of key importance in assessing this potentially efficient hybrid system and especially of interest because SOFC developers are targeting lower operating temperatures to avoid the use of exotic and expensive materials [8]. The novelty of this work is that is studies the integration of these two systems by defining parameters that affect the interaction between the two systems, vary these parameters and analyze their effect on the key performance characteristics of a SSHS.

To identify the key characteristics of a SSHS this work focuses on the interaction between the two systems. Since both system have been studied separately in other studies, it is outside of the scope of this study to investigate the effects of parameters that only affect one of the two systems.

The remainder of the paper is structured the following way:

- Section 2 describes the SSHS in more detail and discusses the thermodynamic model.
- The electrochemical model is validated in Section 3.
- Different cases are studied in Section 4. These cases are chosen to examine the effect of several design choices on the interaction between the SOFC system and the sCO_2 Brayton cycle.
- The paper ends with conclusions and recommendations in Section 5.

2. Thermodynamic operation and model

The goal of this section is to explain the concepts of each system separately and the integration between the two. Furthermore, the thermodynamic model that is base for the case studies is discussed.

2.1. General assumptions

Before getting into the specifics of the two systems, the following general assumptions are made for the thermodynamic model:

- All components are perfectly thermally insulated, therefore there is no heat transfer with the environment
- Fluid properties are taken from Lemmon et al. [20] if temperature and pressure are within range of the database
- When temperature and pressure are out of range for Lemmon et al. [20], the properties are determined by the GasMix method. The GasMix method applies the ideal gas law and temperature dependent specific heats

$$C_P = C_1 + C_2 T + C_3 T^2 + C_4 T^3 \quad (1)$$

Table 1
Overview of selected studies reviewed by Buonomano et al. [9].

	Reforming system	SOFC hybrid setup	TIT(°C)	Turbine PR	Efficiency[a]
Calise et al. [10]	DIR/Anode recirculation	Direct	1250	7.8	67.5%
Chan et al. [11]	DIR/Anode recirculation	Direct	1193	4.58	62.2%
Chan et al. [12]	DIR/HRSG	Direct	948	3.71	61.9%
Song et al. [13]	IIR/Anode recirculation	Direct	840	2.9	60.2%
Jia et al. [14]	DIR/HRSG	None			49%
		Direct	998	2.87	60.65%
		Direct + Rankine cycle	965/340	2.83/254	60.40%
Yang et al. [15]	IIR/Anode recirculation	Direct	750–1150	3.5	42%–70%
	ER/Anode recirculation		750–1150	3.5	32%–60%
Arsalis [16]	DIR/Anode recirculation	Direct + Rankine cycle			66%–74%
Park and Kim [17]	IIR/Anode recirculation	Direct	700–1350	3.5–10.5	55%–72%
		Indirect air Brayton cycle	600–1050	3.5–10.5	47%–66%
Facchinetti et al. [18]	ER/HRSG	Anode coupling[b]	800/1200	2.4/2.3	66.0/68.0%
	ER/HRSG	Cathode coupling[c]	800/1200	5.0/5.5	63.8/65.5%

[a]Electric system efficiency.
[b]The outlet of anode is connected to a compressor and turbine, the fuel cell operates at ambient pressure.
[c]The outlet of cathode is connected to a compressor and turbine, the fuel cell operates at ambient pressure.

Constants are from Chase [21] and are valid from 300 to 5000 K. Switching in methods is done by calculating relative thermodynamic properties, such as the enthalpy and entropy, for both methods with the same temperature. In order to match the thermodynamic values, the switch is done in temperature ranges where both methods are valid.
- The fuel supplied to the SOFC system is pure methane
- Components are modeled by a lumped parameter approach
- A reference environment, standard air, is defined used. See Eqs. (A.1)–(A.3) for more detail.

2.2. The solid oxide fuel cell system

Fig. 3 shows the key components of the SOFC system. Two main processes take place in a SOFC system fed by methane. The reforming and electrochemical process.

The amount of flue gas and its compisition are key in understandig the thermodynamic coupling between the two systems. Therefore, tthe operation of the SOFC system is modelled in detail as described in the following sections.

2.2.1. Reforming process

Pure methane is fed to the SOFC system. However, this cannot be converted to power by the SOFC. In order for the SOFC to work, it needs hydrogen. Therefore, methane is converted to hydrogen or hydrogen co-mixtures in the reformer and the fuel cell.

This process consists of two reactions, the strongly endothermic methane steam reforming (MSR) reaction:

$$CH_4 + H_2O \leftrightarrows CO + 3H_2 \tag{2}$$

And additional hydrogen is formed in the exothermic water-gas shift (WGS) reaction:

$$CO + H_2O \leftrightarrows CO_2 + H_2 \tag{3}$$

The MSR reaction only takes place in the presence of a catalyst around the operating temperatures of 600 to 1000 °C. In case of an IIR setup, the MSR reaction only takes place in the reformer. The WGS takes place without a catalyst, so in case of an IIR setup in both the reformer and anode [22].

As mentioned before, the reforming process is endothermic. Excess heat from the fuel cell drives the process. In this paper, only IIR is considered because of its high efficiency and the fact that it does not suffer from problems typically associated with a DIR system, such as carbon deposition and thermal management [23].

As can be seen, steam is required for this reactions to take place. Steam can either be supplied by recirculating part of the exhaust of the anode flow or by a separate HRSG attached to the outlet of the SOFC. When recirculating part of the anode flow, steam produced in the anode half reaction is supplied to the reformer. This paper only considers anode recirculation since this is a simpler system, more efficient and more common (Table 1).

In order to model the reforming process, the following assumptions are made:

- The outlet of the reformer is the chemical equilibrium of the MSR- and WGS reaction [22];
- The outlet of the anode is the chemical equilibrium of the WGS;
- The equilibrium constants are temperature dependent [24] (see Table A.2);

$$\log K = C_1 + C_2T + C_3T^2 + C_4T^3 + C_5T^4 \tag{4}$$

- The reformer is at a constant temperature. This follows from the lumped parameter approach;
- The steam to carbon ratio at the inlet of the reformer is 1.7 [22].

$$S/C = \frac{\dot{n}_{rf,E}^{H_2O}}{\dot{n}_{rf,E}^{CH_4}} \tag{5}$$

2.2.2. Electrochemical operation

In the fuel cell itself, hydrogen is oxidized and reacts to water. This electrochemical reaction consists of two half reactions, the anode- and cathode half reactions. The electron that is formed in the anode half reaction is not conducted by the electrolyte. It flows through an external electrical circuit to the cathode where it reacts with the oxygen in the air to oxygen ions.

The electrons flowing through the external electrical circuit supply power to an electrical load.[1] The current is determined by the amount of electrons that would flow through the electrical circuit if all combustible products in the syngas, hydrogen, carbon monoxide and oxygen, would be consumed and the fuel utilization ratio:

$$I = U_f 2F(\dot{n}_{rf,L}^{H_2} + 4\dot{n}_{rf,L}^{CH_4} + \dot{n}_{rf,L}^{CO}) \tag{6}$$

The fuel utilization ratio is assumed to be constant at 85% [25].

[1] In this paper, the electrical load is an DC/AC converter which has an efficiency of 97% [25].

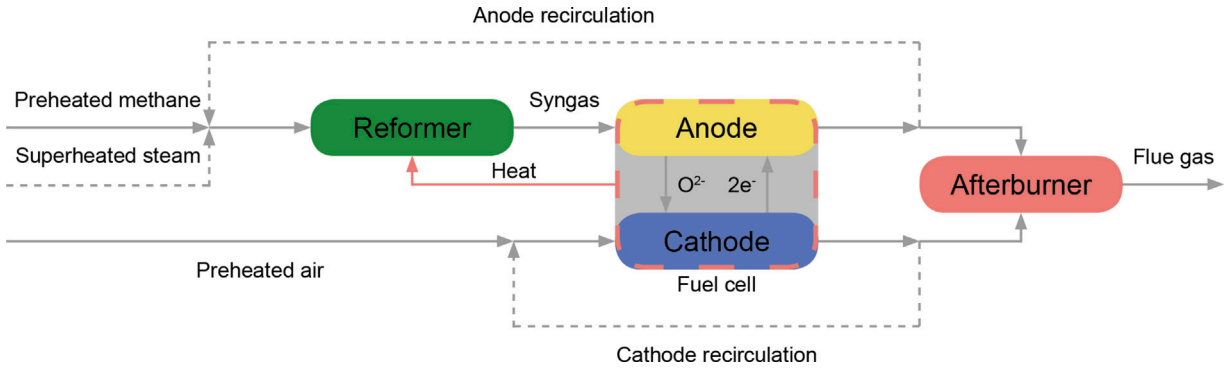

Fig. 3. SOFC system concept.

The ideal potential is determined by the Nernst equation, Eq. (7) [1].

$$E_N = -\frac{\Delta G^0(T_{FC}, P_0)}{2F} + \frac{\tilde{R}T_{FC}}{2F} \ln \frac{P_{H_2}\sqrt{P_{O_2}}}{P_{H_2O}} \tag{7}$$

The partial pressure of each component, used in the Nernst equation, is determined by Raoult's law [26]. This law states that the partial pressure of a component is proportional to its concentration.

Since a lumped parameter approach is applied, the temperature of the SOFC, the current density and potential are constant across the fuel cell.

The actual potential is not the ideal potential. Three mechanisms cause losses: Ohmic-, concentration- and activation overpotential.

Concentration overpotential only becomes significant when the limiting current density is approached [27]. It is assumed that the fuel cell is operated far from this limiting current density. Therefore concentration overpotential is neglected.

Activation overpotential in high temperature fuel cells is very insignificant [27] and therefore neglected.

Therefore, ohmic overpotential is the only loss considered to be relevant. It is highly dependent on the geometry of the fuel cell and its temperature. For stationary power production, ease of scaling up is important. Therefore a cathode supported tubular model is chosen [28]. Table A.1 shows the dimensioning of the components. Since a tubular model geometry is assumed the ohmic resistance is modeled by a circular equivalent electrical circuit as depicted in Fig. 4.

Each ohmic resistance depends on the resistivity of the component, surface and the path length of the electron (Eq. (8)) [29].

$$R^k = \frac{\delta^k \rho^k}{A^k} \tag{8}$$

The resistivity is temperature dependent (Eq. (9)) [30] (see Table A.3).

$$\rho^k = C_1 \exp \frac{C_2}{T_{FC}} \tag{9}$$

2.2.3. Mass and energy balance

Not all chemical energy in the fuel is converted to electricity. A significant part is converted to heat. So the fuel cell has to be cooled. However, it can't be cooled with air of ambient temperature. The fuel and air that enter the SOFC must be preheated to prevent large temperature differences in the fuel cell. Large temperature differences cause thermal stresses that will damage the fuel cell [1]. Consequently, in order to cool the fuel cell, far more air than the stoichiometric ratio is supplied to the cathode.

It is assumed that the entering temperature of both the anode and cathode flow are equal, the temperature in the flows increases by 100 °C and the temperature of SOFC is halfway between the entering and leaving temperatures [31].

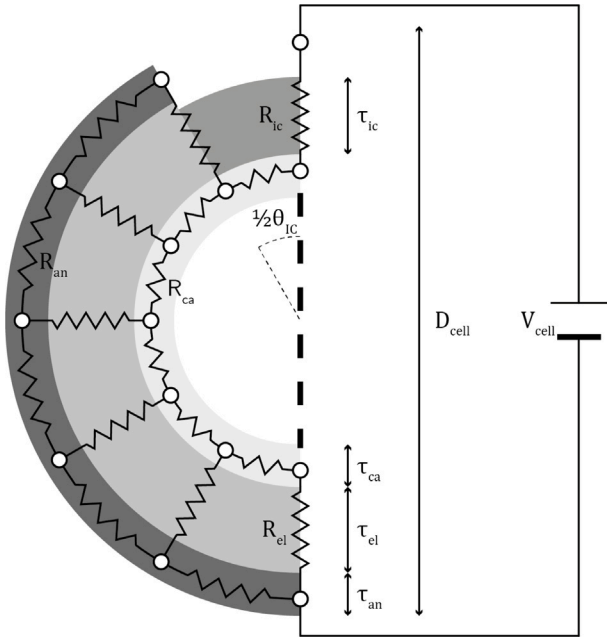

Fig. 4. Equivalent electrical circuit operation.

To determine how much air is needed to cool the fuel cell, the energy balance of the fuel cell must be solved.

$$\dot{m}_{an,E} h_{an,E} + \dot{m}_{ca,E} h_{ca,E} = \dot{W}_{FC,e} + \dot{Q}_{rf} + \dot{m}_{an,L} h_{an,L} + \dot{m}_{ca,L} h_{ca,L} \tag{10}$$

Furthermore, the mass balance must be solved. Specifically the mass balance of the cathode.

$$x_{air}^{O_2} \dot{m}_{air,pre,L} + r_{ca} x_{ca,L}^{O_2} \dot{m}_{ca,L} = \frac{I}{4F} + x_{ca,L}^{O_2} \dot{m}_{ca,L} \tag{11}$$

This is because oxygen from the cathode is transferred to the anode and the fact that the oxygen concentration has an effect on the energy balance of the fuel cell via its effect on the Nernst potential (see Eq. (7)).

2.3. The sCO_2 brayton cycle

Two cycle setups are considered, the simple recuperative cycle and the recompression cycle. The recompression cycle has received the most attention for its relative simplicity and high efficiency [2,3,6,32–34]. Fig. 5 shows the simple recuperative cycle. In the simple recuperative cycle, sCO_2 is compressed from 80 bar, 32 °C (point 1) to 250 bar, 65 °C (point 2). Heat is recovered from the low pressure (LP) flow in the recuperator. This heats the high pressure (HP) flow from point 2 to 3 and cools down the LP flow from the outlet of the turbine (point 5) to the inlet of the cooler (point 6). Finally, heat is added to the cycle,

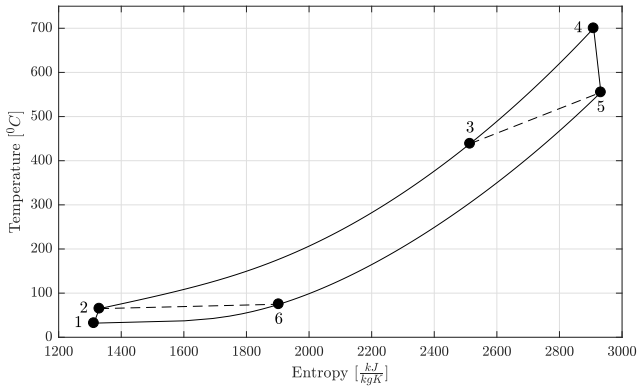

Fig. 5. Temperature-entropy diagram of the simple recuperative sCO_2 cycle (ΔT_{hex} = 10 °C).

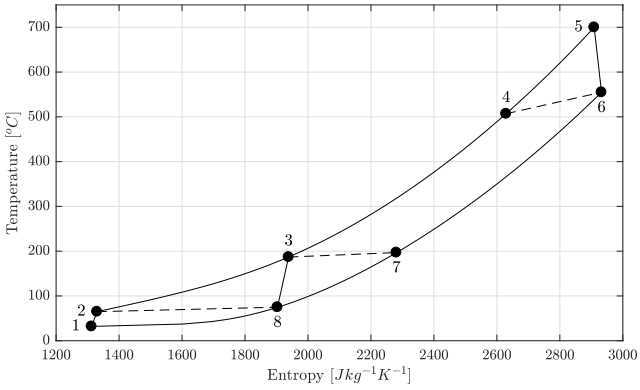

Fig. 6. Temperature - entropy diagram of the recompression sCO_2 Brayton cycle (ΔT_{hex} = 10 °C).

bringing the temperature up to the TIT, limited by the material and construction of the turbine, of 700 °C (point 4) [35].

In the recompression cycle, Fig. 6, part of the flow is compressed at a higher temperature, adding a compressor (point 8 to point 3). This also splits the recuperator into a low temperature (LT) recuperator (point 7, 8, 2 and 3) and a high temperature (HT) recuperator (point 6, 7, 3 and 4). Consequently more heat can be recovered which raises the temperature of point 4 compared to a simple recuperative cycle. Therefore, less heat is required to bring the same amount of sCO_2 up to the TIT. When keeping the same TIT of 700 °C the mass flow can increased. This increases the produced power by the turbine. The additional work of compressing sCO_2 at a higher temperature partly off-sets this gain, but overall the efficiency increases.

Heat is supplied to the sCO_2 Brayton cycle by integrating it with the SOFC system and utilizing its waste heat. The operating conditions of the turbomachinery define part of the boundary conditions for the integration of the two systems. Section 2.4.1 covers the heat exchange between both systems.

Assumptions regarding the turbomachinery:

- The minimum pressure and temperature, the inlet of the compressor, of the cycle is slightly above the critical point at 80 bar and 32 °C to take maximum advantage from the reduced compression work close to the critical point [2].
- A higher pressure and temperature at the inlet of the turbine increase the efficiency of the cycle. The increase in efficiency of a higher pressure becomes limited at a pressure of more than 250 bar [2]. Therefore the maximum pressure of the cycle is assumed at 250 bar.
- The maximum temperature of the cycle is 700 °C. This corresponds to the maximum TIT mentioned before [35].
- Isentropic efficiency of a compressor is 80% and assumed to be constant for all operating conditions [36]
- Isentropic efficiency of a turbine is 90% and assumed to be constant for all operating conditions [35]
- Efficiency of the generator is 95% and assumed to be constant for all operating conditions [37]
- Mechanical losses in the shaft are assumed to be negligible.

It's outside the scope of this work to study the effects of these assumptions.

2.4. Thermodynamic coupling

2.4.1. Heat exchangers

Two types of heat exchangers are used. For the LP flows a common shell and tube heat exchanger (STHE) is used [38]. The HP, HT flows of the sCO_2 require a different type of heat exchanger, a printed circuit heat exchanger (PCHE). This is a compact and highly efficient heat exchanger capable of operating at very high temperatures and pressures (up to 1160 K and 650 bar) [39,40].

The size of the heat exchangers is determined by Eq. (12) [41]. By integrating this equation numerically, the non-constant specific heats of the fluids are taken into account, which is specifically the case for sCO_2 near the critical point.

$$A = \int_0^X \frac{d\dot{Q}}{\bar{U}(T_H(x) - T_C(x))} dL \tag{12}$$

Work on estimating the heat transfer coefficient of a PCHE has been limited so far, is uncertain at best and only suitable for a sCO_2 recuperator [32,40,42]. The goal of this work is to compare different setups with one another, not designing an actual system. It is therefore outside the scope of this study to consider this in detail. Constant heat transfer coefficients based on specifications of the manufacturer [39] and literature [41,43] are used (see Table A.4).

The above equation is solved numerically. The more nodes are used in the discretization, the more accurate the calculation will be. Especially near the critical point this is important , since this is where thermodynamic properties change the most. The effect of the number of cells and the accuracy has been evaluated for a sCO2 cooler, most near to the critical point. After 10 nodes the result converges. To be on the safe side, 20 nodes are used in this work.

2.4.2. Balance of plant

Finally, some basic balance of plant (BoP) elements are modeled.

In the afterburner the mix of the anode and cathode exhaust is combusted. Complete combustion of methane, carbon monoxide and hydrogen is assumed.

To simplify the design process of a heat exchanger network, a pressure drop is assumed that does not depend on the heat exchangers it flows through. Instead, each flow, hot and cold, has an assumed relative pressure drop. It's outside the scope of this work to model pressure drop more accurrately because it does not have a significant effect on the integration of the two systems.

This pressure drop is linearly related to the change in enthalpy of a flow. For example, a cold flow like the fuel that has to be preheated, drops 50% of the specified pressure drop (50% of 2% in this case) when 50% of the required heat is added.

Furthermore, a relative pressure drop is assumed in the fuel cell, reformer and afterburner. Mixing and splitting of flows is assumed to cause no pressure drop (see Table 2).

3. Electrochemical model validation

This section discusses the validation of the electrochemical model of the SOFC as described in Section 2.2. The results of this model of the fuel cell are compared to other models found in research literature in Section 3.1 and to experimental data in Section 3.2.

Table 2
Pressure drop in different components.

	Pressure drop (%)
Cold/Hot flows	2 [32]
Fuel cell/reformer	4 [37]
Afterburner	5 [37]
Mixing/splitting	0

Table 3
Comparison between the model and measured data.

	800 °C	900 °C	1000 °C
Measured area specific resistance (ASR) (Ωcm^2)	1.673	0.9530	0.6342
Model ASR (Ωcm^2)	1.416	0.925	0.656
Difference (%)	−15.34	−2.89	+3.41

3.1. Comparison with literature

The model of this study is compared to other similar models. A summary of the comparisons is given in Tables C.7–C.11.

In general, it can be concluded that the developed model in this study performs well when compared to other works. Concentration of components of the syngas do differ slightly in some comparisons but not to such an extent that it is reason for concern. The small differences can be explained by slightly different modeling approaches and assumptions.

The overall performance of the cell differs very little in most comparisons. Compared to work from Campanari and Iora [29] the ohmic overpotential is between 2.5 and 5% lower, the concentration of the components in the syngas matches nearly perfectly but the power density is around 7% higher.

Compared to work from Chan et al. [11], the efficiency is slightly significantly higher. However, when compared to Asimptote [44] the overall efficiency is slightly lower.

Compared to work from Aguiar et al. [45] and Aguiar et al. [46], the concentration of the components in the syngas does deviate but the overall efficiency of the fuel cell matches well.

These differences are not considered significant enough to adjust the model.

3.2. Comparison with experimental data

The results of the model are compared to measured data from a typical tubular SOFC [47]. The ASR is compared as a function of temperature.[2] Table 3 shows that the model has a higher voltage than the test data does. One reason is that the model neglects activation and concentration losses. Another is that in case of 800 and 900 °C, the ohmic resistance is modeled lower than it is in the test.

A reason for this deviation is that in reality the temperature of the fuel cell itself is probably not constant. This causes the ohmic resistance to vary along the cells length. In the model, the ohmic resistance is approached by assuming an average stack temperature. Finally, the temperature dependence of the specific resistivity of the components is an approximation as well.

The difference between the model and tested data is in some cases quite significant. However, these deviations can be explained (at least partly). The comparison does confirm however that the model shows a performance in the same order of magnitude. In combination with the fact that the model performs comparable to other models in research literature there is enough reason to validate the model for its purpose.

4. Case studies

Four different cases of the SSHS are considered in this paper (and a directly coupled GT as reference). Each case is chosen to analyze a specific concept.

Firstly, a base case is defined, case I, Section 4.1. This layout is the SSHS in its simplest form. A simple recuperative sCO_2 Brayton cycle is coupled to the SOFC system with one heat exchanger. The other three cases in this paper are chosen to illustrate the effect of several design parameters. Each case, except case V, is more efficient than the last but also more complex, demonstrating the trade-offs of a SSHS.

- Case II, Section 4.2, introduces the concept of cathode recirculation. This new design parameter is studied and an optimal case is defined.
- Case III, Section 4.3, discusses the pro's and cons of a pinch point optimization by applying this to case II.[3]
- Case IV, Section 4.4, explores what effect having a recompression cycle in stead of a simple recuperative cycle has on the SSHS. When introducing the recompression cycle, the minimal temperature difference in the heat exchangers has an effect on the pinch temperature and therefore the design of the heat exchanger network.
- Finally, case V, Section 4.5, briefly discusses a hybrid system with a directly coupled GT to the SOFC system for comparison.

These cases are highlights chosen from a more extensive case study analysis by Schöffer et al. [48].

This section ends with a comparison between the cases is in Section 4.6.

Part of the operating conditions and characteristics are the same for each case:

- All setups are considered for a fuel feed of pure methane, $1\,mol\,s^{-1}$
- The current density. This results in a same number of cells for each setup as well.
- In all setups the operating temperature of the SOFC is at 836.85 °C. Therefore, since it is assumed that the in- and outlet temperature of the SOFC are 50 °C lower and higher than its operating temperature, the outlet temperature equals the maximum operating temperature of the PCHE (1160 K/886.85 °C). This is done to take advantage of the decreasing ohmic resistance with increasing temperature as much as possible. This outweighs the reduction of the Nernst voltage as a consequence of a higher temperature and therefore has a positive effect on the performance of the SOFC. It is also because of this that the afterburner is placed downstream of the afterburner. This cools down the flue gas before increasing it again to the maximum temperature.

Figs. 8, 9, 11, 17 and 18 schematically show the heat exchanger network of different cases. In these figures, the process streams that need to be heated are the blue arrows from right to left. The streams that need to be cooled are the red arrows from left to right. These streams are connected by heat exchangers which are marked by a tag as well. Heat is rejected to the environment by exhausting flue gas or cooling sCO_2 with water. For example, in Fig. 8 heat exchanger A1 transfers heat from the hot flue gas to the cold air. And heat exchanger C1 cools the sCO_2 by rejecting it to the environment (via cooling water).

[2] The ASR of the test data is an approximation based on the test data.

[3] A simple example of a pinch analysis can be found in Appendix B.

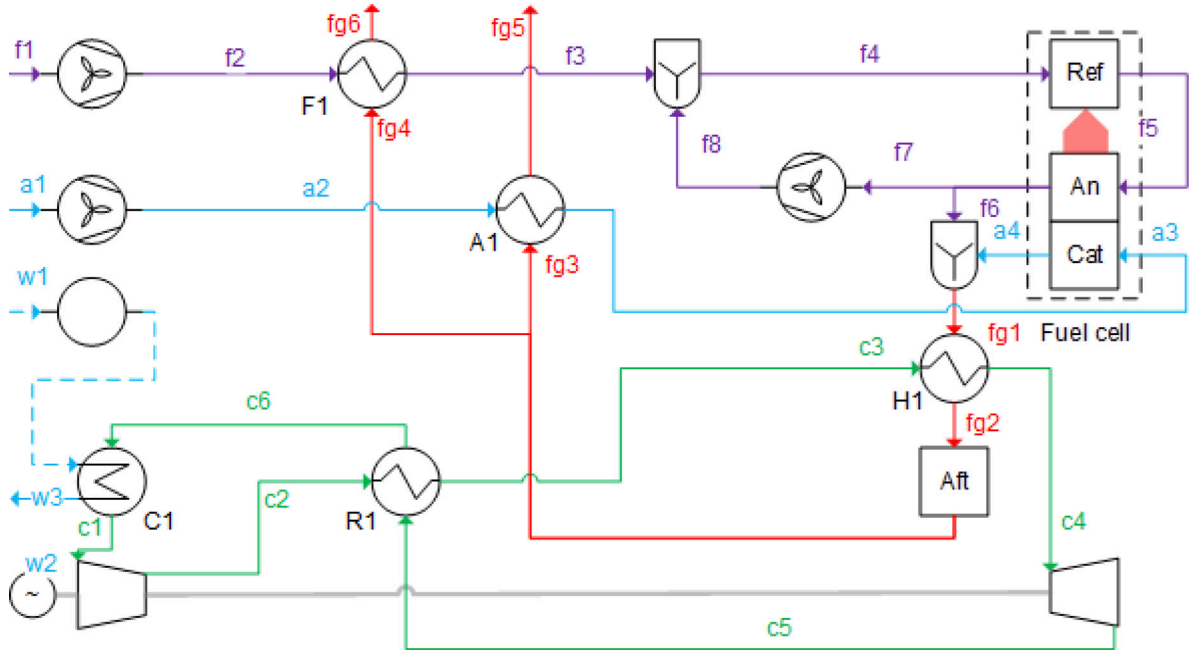

Fig. 7. PFD (Case I: Base case (purple (f) = fuel (methane), blue (a) = air, green (c) = sCO_2, red (fg) = flue gas, dashed blue (w) is cooling water)). (For interpretation of the references to colour in this figure legend, the reader is referred to the web version of this article.)

Table 4
Key performance data (Case I: Base case, $\Delta T_{hex} = 10\,°C$).

Fuel cell power	380 kW
Generator power	155 kW
Auxiliary power consumption	53 kW
Net AC system power	482 kW
LHV AC efficiency	60.01%
Thermodynamic cycle efficiency	43.16%
sCO_2 cycle flow	26.1 mol s^{-1}
Total PCHE area	29 m^2
Total STHE area	8109 m^2
Number of heat exchangers	5

4.1. Case i: Base case

To establish a base line, the most simple setup is considered first. The excess heat of the SOFC system is transfered by one heat exchanger to the sCO_2 cycle. Fig. 7 shows that the exhaust gas of the anode that is not recirculated mixes with the exhaust of the cathode and is used to supply heat to the sCO_2 cycle.

After this, the flue gas is combusted in the afterburner. It is not combusted right after the SOFC because this would increase the temperature to above the design temperature of the PCHE.

The temperature at point *fg2* is chosen in such a way the temperature at point *fg3* and *fg4* is slightly higher than point *a3*.

$$T_{aft,L} = T_{ca,E} + \Delta T_{hex,min} \tag{13}$$

The temperature difference in a heat exchanger is a trade-off between efficiency and costs. An optimum is commonly found between 10 and 30 °C [38]. In this case, 10 °C is assumed to assess the most efficient system within this range. A higher temperature will decrease the size of heat exchangers and efficieny but not the integration of the two systems qualitatively. Table 4 shows the key characteristics of case I and Table 7 shows the key performance data for this and all other cases.

The advantage of this case is its relative simplicity. The drawbacks are the fact that not all excess heat is transferred to the power cycle and the large air preheater (STHE A1 in Fig. 8) due to the relatively low temperature difference (driving force). Furthermore, the heat that is transferred to the cycle can be converted to power more efficiently by applying a recompression cycle. These three *issues* will each be addressed in the following three cases.

4.2. Case II: Cathode recirculation

In order to decrease the size of the air preheaters the exhaust of the cathode can be recirculated. Before mixing the exhaust of the cathode with that of the anode, the outlet of the cathode is split. Part of the exhaust is mixed with the outlet of the air preheater. Fig. 3 shows this schematically. The PFD in Fig. D.3 shows that compared to case I, the outlet of the cathode is split, an air mixer downstream of the air preheater is added and a fan upstream of this mixer. However, as Fig. 8 shows, the design of the heat exchanger network remains the same. It is only the temperatures of the inlet of the air mixer and the in- and outlet of the afterburner and the mass flows that change.

This has effect on several performance characteristics.

Firstly, since the mass flow in the air preheater (A1) and the outlet temperature decrease, the heat exchanger becomes significantly smaller, see Fig. 9. The total size of the PCHE increases because the inlet temperature of the afterburner increases and therefore the temperature difference at the LT end of the heater (H1) decreases.

Furthermore, more heat is transfered to the sCO_2 Brayton cycle. This can be understood by the fact that more heat is transfered to the air flow directly which leads to more available excess heat. This is reflected in the increasing mass flow in the sCO_2 cycle. This also increases the overall efficiency. The increasing mass flow in the sCO_2 cycle increases the power produced by the generator (the other operating conditions remain constant) and the performance of the SOFC is only slightly effected. This is because of the high equivalence ratio that limits the decrease of the oxygen concentration, as well as the limited effect of the oxygen concentration on the Nernst voltage.

Overall, cathode recirculation ratio has a positive effect. Recirculating more cathodic air has a positive effect up to a certain point. The limiting factor is maintaining a minimal temperature difference in the fuel preheater. For a minimal temperature difference of 10 °C this limit is at a recirculation ratio of 67.39%. Increasing the cathode recirculation ratio more will decrease the outlet temperature of the afterburner to such an extent that the minimal temperature difference

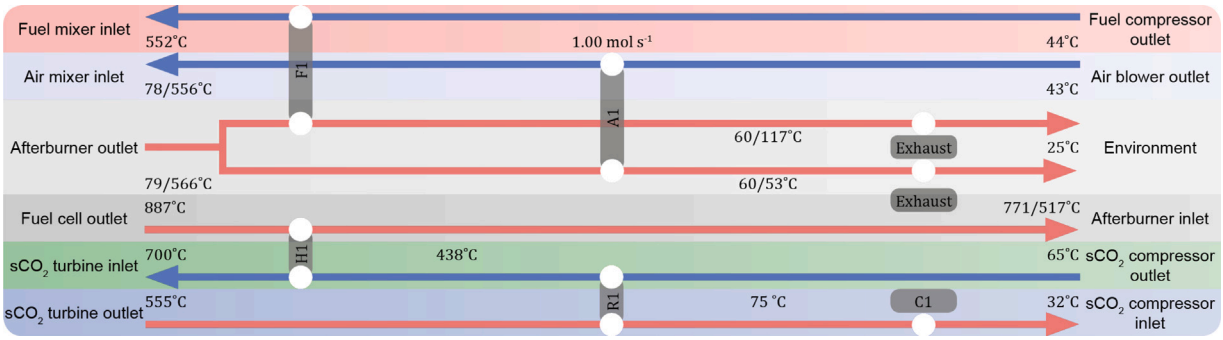

Fig. 8. Heat exchanger network (Case I and II, ΔT_{hex} = 10 °C; temperatures apply to case I/II).

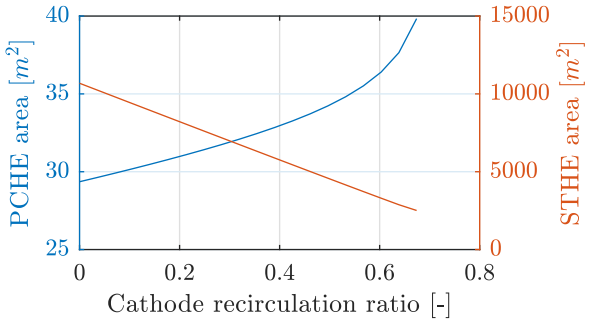

Fig. 9. Heat exchanger area (Case II: Cathode recirculation, ΔT_{hex} = 10 °C). (For interpretation of the references to colour in this figure legend, the reader is referred to the web version of this article.)

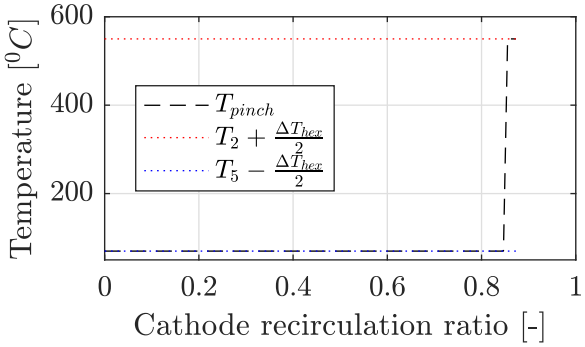

Fig. 10. Relation between the cathode recirculation ratio and pinch temperature (case III: Pinch point optimization, numbered temperatures refer to Fig. 5).

in the fuel preheater is not maintained. Table 7 shows the specifics for these design parameters.

4.3. Case III: Pinch point optimization

In order to maximize the amount of heat that is transfered to the sCO_2 Brayton cycle and minimize the waste of heat a pinch point optimization is applied.

To apply a pinch point optimization in this case means to take a step back in the design process. First, the effect of the cathode recirculation ratio on the pinch temperature is considered. Fig. 10 shows that the pinch temperature either corresponds to the interval temperature of the outlet of the compressor or to the turbine outlet temperature (TOT). In the latter case, at a cathode recirculation ratio of 85.05% or higher, less heat is transfered to the sCO_2 Brayton cycle and the SSHS is less efficient. It is found that this behavior of the pinch temperature is not affected by the minimal temperature difference, therefore a minimal temperature difference of 10 °C is assumed as before.

Next, consider the effect of the cathode recirculation ratio. It has an effect on the design of the heat exchanger network. Table 5 divides this case into 4 sub-cases based on the design of the heat exchanger network. Fig. 11 shows the different designs for sub-case A to C, up to the recirculation ratio where the pinch temperature *jumps*.

Firstly, consider sub-case B compared to case I and II. By applying a pinch optimization, more heat is transfered to the sCO_2 cycle, especially more LT heat from the flue gas. This does however require two

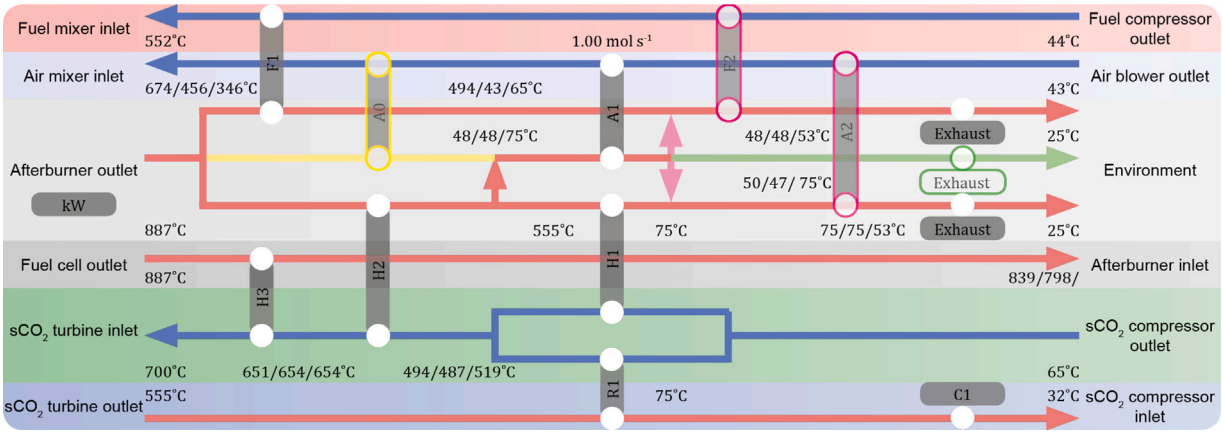

Fig. 11. Heat exchanger networks (case III: Pinch point optimization, ΔT_{hex} = 10 °C, 0% ≤ r_{ca} ≤ 85.04%; heat exchanger A0 (yellow) only applies to sub-case III.A, heat exchangers F2 and A2 (pink) only apply to sub-case III.C, the exhaust in green only applies to sub-case III.A and III.B; temperatures apply to a recirculation ratio of 50/74.86/80%). (For interpretation of the references to colour in this figure legend, the reader is referred to the web version of this article.)

Table 5
Division of heat exchanger network designs (Case III, ΔT_{hex} = 10 °C).

Sub-case	Cathode recirculation ratio (%)	Number of heat exchangers
A	0–73.49	8
B	73.50–74.86	7
C	74.87–85.04	9
D	85.05–87.30	7

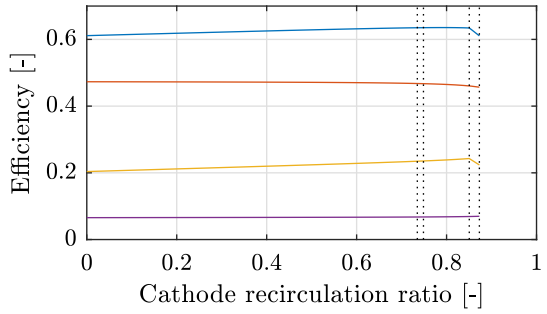

Fig. 12. Power as fraction of LHV of methane (Case III: Cathode recirculation ratio, ΔT_{hex} = 10 °C; From top to bottom: Net system AC power, SOFC power, generator power and auxiliary consumption, division between sub-cases marked by dashed lined).

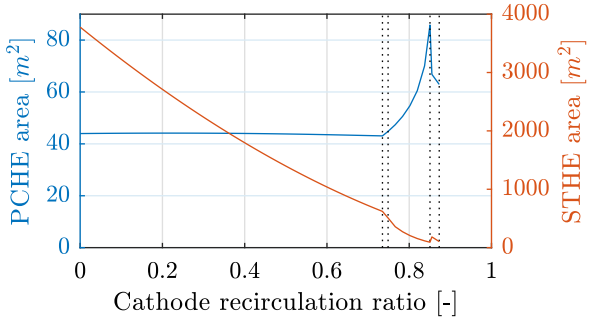

Fig. 13. Effect of the cathode recirculation ratio on the area of the heat exchangers (case III: Cathode recirculation, ΔT_{hex} = 10 °C; division between sub-cases marked by dashed lined.

additional heaters and the LT sCO_2 flow has to be split before entering the recuperator.

Sub-case B only applies to a small cathode recirculation ratio range. Decreasing the recirculation ratio from sub-case B to sub-case A increases the inlet temperature of the air mixer ($T_{mix,E}$). Therefore more HT heat is required to preheat the air feed, which is supplied through and additional heat exchanger, A0, sub-case A.

Increasing the recirculation ratio from sub-case B to sub-case C increases the water content in the flue gas to such an extent that condensation would occur in the air (A1) and fuel (F1) preheater. To avoid this, two additional heaters, one for each, are added to increase the outlet temperature of the flue gas.

Sub-case D has, as mentioned before, a higher pinch temperature and therefore a different heat exchanger network as well. The efficiency however is considerably lower than sub-case A to C. See Fig. D.4 for the heat exchanger network.

Fig. 12 shows that, similar to case II: Cathode recirculation, the efficiency increases when increasing the cathode recirculation ratio. This is true up to case D, where the pinch temperature *jumps* so that it corresponds to the TOT. At this point the efficiency decreases. From this it follows that the upper limit of sub-case C is the most efficient.

Fig. 13 shows that the area of the STHE decreases as the cathode recirculation ratio increases, similar to case II. The area of the PCHE starts to increase from sub-case B and decrease again from sub-case D.

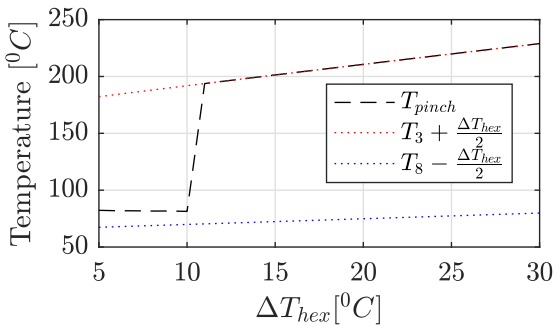

Fig. 14. Relation between the minimum temperature difference and pinch temperature (Case IV, r_{ca} = 0%, numbered temperatures refer to Fig. 6).

Table 6
Division of heat exchanger network designs (Case IV: Recompression cycle, ΔT_{hex} = 15 °C).

Sub-case	Cathode recirculation ratio (%)	Number of heat exchangers
A	0–63.76	10
B	63.77–69.63	9
C	69.64–75.93	10
D	75.94–82.41	9
E	82.42–87.30	8

Even though the upper limit of sub-case C is the most efficient, the two additional heat exchangers compared to sub-case B and the increased PCHE area don't seem to be worth it. Therefore, sub-case B is considered the best of case III and is the only one to be considered further in this paper. More specifically, the upper limit of sub-case B, a recirculation ratio of 74.86%. See Fig. D.5 for a detailed heat exchanger network of this case.

4.4. Case IV: Recompression cycle

Before considering the recompression cycle in combination with cathode recirculation, the effect of only the recompression cycle is considered. Fig. 14 shows the effect of the minimal temperature difference in the heat exchanger network on the pinch temperature. In case of a low minimal temperature differences, the pinch temperature is not directly related to the in- or outlet temperature of one the hot or cold streams. Around 10 °C the pinch temperatures *jumps* and aligns with the outlet temperature of the HT compressor.

This difference in pinch temperature has an effect on the design of the heat exchanger network. Fig. 17 shows the two heat exchanger networks that follow from this. Case IV.2 is more efficient, since the minimal temperature difference is lower, 10 °C, but also more complex. It has one more heat exchanger than case IV.1 (15 °C) and it has a more complex setup in preheating the large airflow. Therefore, case IV.1 is considered the better setup and the effect of cathode recirculation in combination with a recompression cycle is examined for a minimal temperature difference of 15 °C.

Similar to case III, the pinch temperature remains constant up to a certain point, 75.93% in this case. Table 6 shows the five sub-cases which have a qualitatively different design of the heat exchanger network. Fig. 18 shows the different heat exchanger networks for sub-case A to C. Sub-case D and E are not further considered in this because of their much lower efficiencies (see Fig. 15).

Sub-case IV.A has the same design as when no cathode recirculation is applied. This is possible up to a recirculation ratio of 63.77%, at this point the temperatures in the heat exchangers have changed in such a way that it is possible to cut out one fuel preheater (F0) from the design and just use one fuel preheater, sub-case IV.B.

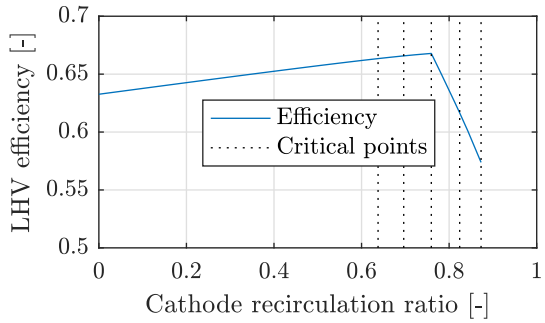

Fig. 15. SSHS efficiency (case IV, ΔT_{hex} = 15 °C).

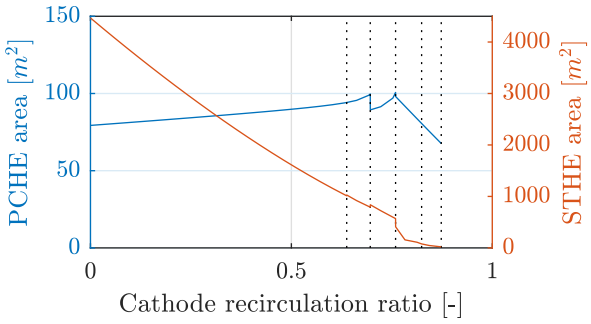

Fig. 16. Effect of the cathode recirculation ratio (Case IV, ΔT_{hex} = 15 °C)).

The upper limit of sub-case IV.B (69.63%) is reached when the temperature difference at the LT end of heat exchanger H3 has decreased to the imposed 15 °C.

Sub-case IV.C solves this problem by adding a heat exchanger (heat exchanger H2.5 on Fig. 18), which makes the system more efficient but also significantly more complex. Sub-case IV.C is possible up to the point where the pinch *jumps*. Fig. 15 that Case IV.C has the highest efficiency. However, as Fig. 18 shows, the heat exchanger network design is more complex compared to case IV.B, which has the second highest efficiency.

Fig. 16 shows that, similar to the other cases, the total area of the STHE significantly decreases if more cathodic air is recirculated. The area of the PCHE increases as the temperature difference become smaller. A significant reduction in the area of both types of heat exchangers is observed when the pinch jumps (75.93%).

The combination of increased efficiency, reduced area of STHEs and a limited increase of the area of the PCHEs makes the upper limit of sub-case IV.B, a recirculation ratio of 69.63%, the most favorable setup. References to case IV in other sections of this paper are to sub-case IV.B specifically unless mentioned otherwise. See Fig. D.6 for the heat exchanger network.

Table 7 shows that this case has the highest efficiency of all even though the minimal temperature difference is higher than in other cases. Furthermore the total area of the STHEs is the second lowest.

However, the total area of the PCHE is more than double as high as the second highest and the this case has the most heat exchangers.

4.5. Case V: Directly coupled GT

As mentioned in Section 1, a setup with a directly coupled GT is considered as well for comparison. Table 1 shows different studies of directly coupled GT setups and varying efficiencies. In order to make a fair comparison, a directly coupled GT is studied under the same operating conditions and assumptions as the SSHS. That means that the isentropic efficiency of the turbomachinery is the same in both cases. On additional parameter, the GT pressure ratio is required. From Yang et al. [15] a pressure ratio of 3.5 is chosen.

Fig. D.7 shows the PFD of the directly coupled GT system. Part of the cathodic air has to be recirculated in order to increase the TOT above the outlet temperature of the air feed. The cathode recirculation ratio is chosen in such a way that the temperature difference at HT end of the air preheater is the imposed minimal temperature difference of 10 °C.

Table 7 shows that the net power produced by this system is very similar to that of case II and III. The PCHEs are not necessary in this system and the total area of STHEs is similar to case II.

Further analysis of this setup is outside of the scope of this study. It only serves as a reference case to compare the different SOFC-sCO_2 Brayton cycle hybrid system setups.

4.6. Comparison

All cases are compared on their efficiency, number of heat exchangers and heat exchanger area of both types, PCHE and STHE. Three effects are compared. Firstly, the effect of recirculating cathodic air, case II, is compared to the basic SOFC setup, case I. Secondly, the effect of a pinch point optimization by comparing case II to III. Thirdly, the performance of the simple recuperative cycle is compared to the recompression cycle by comparing case III and IV. Finally, case II, III and IV are compared to the directly coupled GT setup, case V.

Firstly, consider case I and II to assess the effect of recirculating cathodic air.

Cathode recirculation, case II, increases the performance of the system. Firstly because more heat can be transferred to the sCO_2 Brayton cycle. The reduction of the oxygen concentration in the fuel cell is limited and the performance of the fuel cell is only very slightly affected. Therefore cathode recirculation increases the efficiency of the total system quite significantly. Furthermore, the air preheater becomes significantly smaller. However, recirculating cathodic air does require the outlet flow of the cathode to be split and mixed. This requires a high temperature blower and large mixer, complicating the system. The total area of PCHE is hardly affected.

Secondly, consider case II and III as a comparison of a pinch point optimization.

The efficiency is slightly lower when a simpler design approach (case II) is applied because less heat is transfered to the sCO_2 Brayton cycle. In the simpler approach, case II, two less heater exchangers are required for transferring heat to the sCO_2. This results in a considerably simpler design. The total area of the PCHEs is smaller in case II because less heat is transfered to the sCO_2 and the driving force in the heaters is also larger. However, the total size of the STHEs is more than double that of case III. In case II, the temperature difference at the HT end of the air preheater is only 10 °C, compared to 100 °C in the design of case III. This much smaller driving force, combined with the large heat duty required to preheat the air, leads to a much larger total area of STHEs.

This shows that designing a heat exchanger network along a pinch point optimization instead of a *simple* approach does not only improve efficiency, albeit slightly, but it also greatly reduces the size of the heat exchangers. The increased complexity of the system seems to be worth it, considering the general improvement of the system.

Thirdly, consider case III and IV as a comparison between the simple recuperative cycle, case III, and the recompression cycle, case IV.

The recompression cycle converts heat more efficiently into work, therefore the efficiency of the system also increases. This is still the case even though the minimal temperature difference in IV (15 °C) is higher than in case II (10 °C). An additional recuperator is necessary in the recompression cycle, increasing the area of the PCHEs. Furthermore, the higher pinch temperature linked to the outlet of high temperature compressor (HTC) (Fig. 14) makes it that an additional air preheater is required. These two effects increase the total number of heat exchangers by two. The higher pinch temperature also reduces the driving force in the air preheaters, resulting in a larger area of STHEs even though

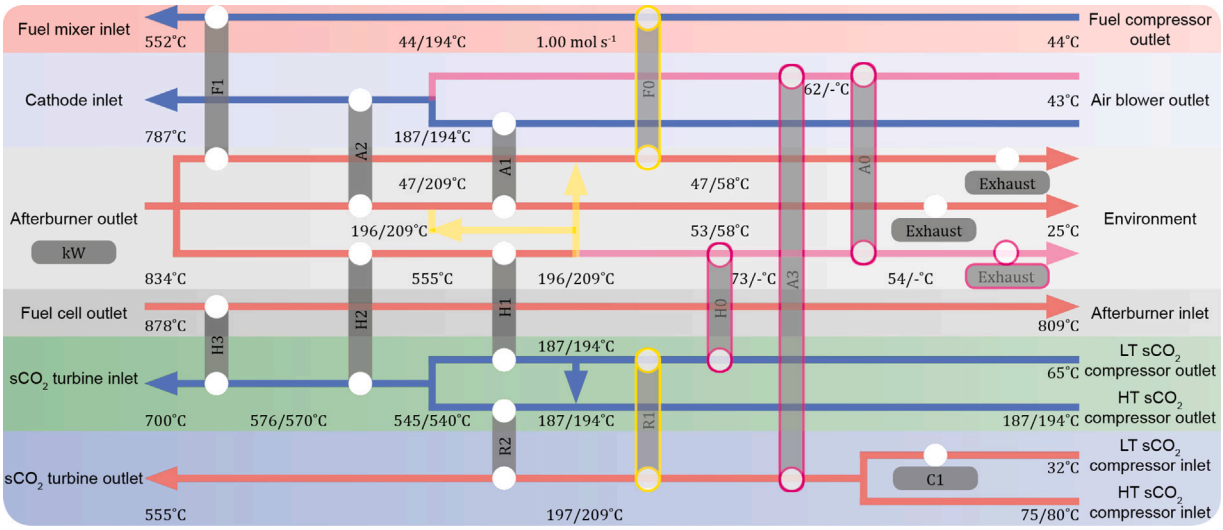

Fig. 17. Heat exchanger networks (Case IV: Recompression cycle, r_{ca} = 0%; heat exchangers R1 and F0 (yellow) only apply to sub-case IV.1 (ΔT_{hex} = 15 °C), heat exchangers H0, A0 and A3 (pink) only apply to sub-case IV.2 (ΔT_{hex} = 10 °C; temperatures apply to case IV.1/IV.2). (For interpretation of the references to colour in this figure legend, the reader is referred to the web version of this article.)

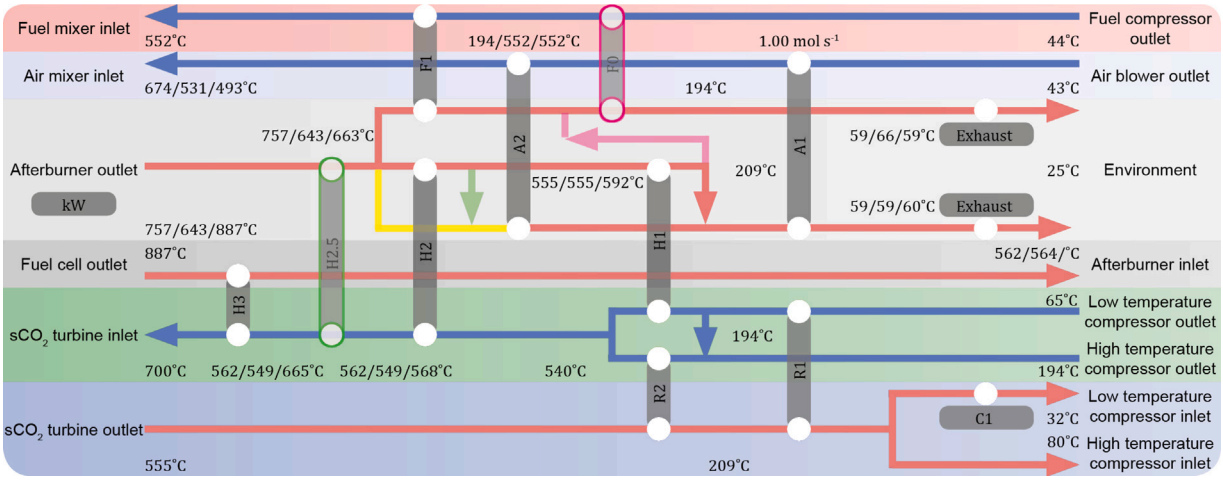

Fig. 18. Heat exchanger networks (Case IV: Recompression cycle, ΔT_{hex} = 15 °C, 0% ≤ r_{ca} ≤ %75.93; yellow applies to sub-case IV.A and IV.B, heat exchanger A0 (pink) only applies to sub-case IV.A and heat exchanger H2.5 (green) only to sub-case IV.C; temperatures apply to a recirculation ratio of 50/69.63/72.5%). (For interpretation of the references to colour in this figure legend, the reader is referred to the web version of this article.)

the recirculation ratio is higher, and thus the heat duty is lower, in case IV compared to case III.

So, a recompression cycle does not only have an effect on the equipment of the sCO_2 Brayton cycle itself, it also complicates and increases the size of the heat exchangers of the SSHS. The efficiency of the SSHS is increased, but not by as much as when the sCO_2 operates as a standalone system. After all, most power is still produced by the SOFC system and the efficiency of the sCO_2 Brayton cycle only has an effect on the conversion of the excess heat to power.

Finally, a comparison is made with the directly coupled GT.

Table 7 shows that all cases, except case I, of the SSHS have a similar efficiency compared to the directly coupled GT. However, this comes at a price. The total number of heat exchangers increases significantly and a PCHE is necessary.

5. Conclusions and recommendations

5.1. Conclusions

This study has explored several design concepts of a solid oxide fuel cell- supercritical carbon dioxide Brayton cycle hybrid system. All concepts show efficiencies in the same range, but differ quite significantly in the design and total size of the heat exchanger network. Designing a solid oxide fuel cell- supercritical carbon dioxide Brayton cycle hybrid system is not simply a matter of picking the setup with the highest efficiency. It is a trade off between system complexity, size of the heat exchangers and system efficiency.

Designing a solid oxide fuel cell- supercritical carbon dioxide Brayton cycle hybrid system along the line of a pinch point optimization or a simpler approach illustrates this trade off. A pinch point optimization increases the efficiency but also the complexity of the system. With more knowledge of practical operation and components cost an optimized design can be found.

Table 7
Comparison of considered cases.

	Case				
	I: Base	II: Cathode recirculation	III: Pinch analysis	IV: Recompression cycle	V: Directly coupled GT
Power (kW)					
Fuel cell	380	377	375	376	372
Generator	155	185	189	212	186
Auxiliary consumption	53	54	54	54	39
Net system AC	482	507	510	534	519
LHV AC efficiency (%)	60.01	63.20	63.52	66.58	64.75
sCO_2 Brayton cycle					
Efficiency (%)	43.16	43.16	43.16	49.68	–
Mass flow ($mol\,s^{-1}$)	26.1	31.1	31.8	41.4	–
PCHE areas (m^2)					
PCHE H1	3.0	8.4	3.1	7.8	–
PCHE H2	–	–	4.3	1.0	–
PCHE H3	–	–	1.0	10.0	–
PCHE R1	15.2	18.1	22.7	22.2	–
PCHE R2	–	–	–	47.4	–
PCHE C1	11.2	13.4	13.7	11.3	–
Total	29.4	39.9	44.8	99.7	–
STHE areas (m^2)					
STHE A1	8090	2430	488	428	2759
STHE A2	–	–	–	317	–
STHE F1	19	80	20	47	34
Total	8109	2510	508	792	2793
Total amount of hex	5	5	7	9	2

The differences between the cases are mainly in the design of the heat exchanger network and size of the heat exchangers, less in their efficiency. The recompression cycle clearly demonstrates this. Applying it does not only add a recuperator and compressor to the system, it complicates the solid oxide fuel cell- supercritical carbon dioxide Brayton cycle hybrid system as a whole.

Cathode recirculation clearly is preferable from a thermodynamic point of view as well from the point of view of the number and size of heat exchangers. However, it does require a blower at high temperatures and a large mixer.

Depending on which design criteria are most important, one of the folllowing setups should be considered. For the highest efficiency, a recompression cycle in combination with a pinch point optimzation is the best option. For the smallest heat exchangers, a simple recuperative cycle in combination with a pinch point optimization is the best. For a relatively simple system, a simple recuperative cycle without a pinch point optimization is the best option.

Compared to a more simple, directly coupled gas turbine, the solid oxide fuel cell- supercritical carbon dioxide Brayton cycle hybrid system:

- Shows similar efficiencies. Keeping in mind that the case for the directly coupled gas turbine is not optimized;
- Is potentially easier to operate.

For an indirectly coupled system, such as the solid oxide fuel cell- supercritical carbon dioxide Brayton cycle hybrid system, this is remarkable since these systems are generally less efficient than directly coupled systems. If it is indeed easier to operate is not clear yet. The high operating pressures of the supercritical carbon dioxide Brayton cycle, the not so straightforward design of the heat exchanger network, the required mixers and necessary high temperature blowers involved make it hard to judge at this point.

5.2. Recommendations

Since the main potential of this system is its potential ease of operation compared to a directly coupled system, this is what future research and practice should be focused on. Practical feasibility of cathode recirculation and off-design operation should be investigated in order to determine if a solid oxide fuel cell- supercritical carbon dioxide Brayton cycle hybrid system has a future.

Off-design operation is especially important when taking into consideration that increased production by renewable energy sources requires more flexibility from other sources. Therefore it is important to analyze the turbomachinery in part-load operation, thermal management of the fuel cell and the possibility to easily start and stop the system completely.

Also, it seems likely that a lower operating temperature of the solid oxide fuel cell will benefit the integration of the two systems. In this study, the flue gas is first cooled down before the temperature is increased again in the afterburner so that it doesn't exceed the maximum temperature of the heat exchangers. Lowering the outlet temperature of the solid oxide fuel cell would eliminate this extra step and fits well with the development towards lower temperature solid oxide fuel cell's.

Furthermore, all components in this system, the solid oxide fuel cell, the supercritical carbon dioxide turbomachinery and the printed circuit heat exchanger, are all relatively undeveloped and expensive technologies. The potential advantages of this system might not outweigh the probable high costs. A cost estimation would therefore be valuable.

Finally, the operating conditions of the simple recupartive cycle and recompression cycle are constant in this work. A sensitivity analysis on these conditions is recommended to fully understand the integration between the two systems.

CRediT authorship contribution statement

S.I. Schöffer: Methodology, Software, Formal analysis, Writing - original draft, Visualization. **S.A. Klein:** Conceptualization, Validation, Writing - review & editing, Supervision. **P.V. Aravind:** Conceptualization, Validation, Writing - review & editing. **R. Pecnik:** Conceptualization, Validation, Writing - review & editing.

Appendix A. Additional data and equations for thermodynamic model

$$T_0 = 298.15\,\mathrm{K} \tag{A.1}$$

Table A.1
Component sizes of a tubular cell.

Cell length	150 cm [27]
Cell outer diameter	2.2 cm [27]
Cathode thickness	2 mm [27]
Electrolyte thickness	40 μm [27]
Anode thickness	150 μm [27]
Interconnection thickness	100 μm [27]
Interconnection angle	30° [30]

Table A.2
Constants for Eq. (4) [24].

	MSR reaction	WGS reaction
C_1	$1.950\,28 \times 10^{-1}$	-3.915×10^{-2}
C_2	$-2.252\,32 \times 10^{-4}$	$4.637\,42 \times 10^{-5}$
C_3	$1.240\,65 \times 10^{-7}$	$-2.574\,79 \times 10^{-8}$
C_4	$-2.631\,21 \times 10^{-11}$	$5.473\,01 \times 10^{-12}$
C_5	-66.1395	13.2097

Table A.3
Constants for Eq. (9) [30].

	C_1 (Ωcm)	C_2 (K)
Anode	2.98×10^{-3}	-1392
Cathode	8.114×10^{-3}	600
Electrolyte	2.94×10^{-3}	10350
Interconnect	1.256×10^{-1}	4690

Table A.4
Estimated overall heat transfer coefficients.

	$\bar{U}$ (W m^{-2} K^{-1})
PCHE recuperator (sCO_2 to sCO_2)	754
PCHE heater (flue gas to sCO_2)	500
PCHE cooler (sCO_2 to water)	7000
STHE gas to gas	20
STHE gas to water	30

$$P_0 = 1.013\,25\,\text{bar} \tag{A.2}$$

$$[x_0^{N_2}, x_0^{O_2}, x_0^{H_2O}, x_0^{CO_2}] = [0.7649, 0.2035, 0.0313, 0.0003] \tag{A.3}$$

Appendix B. Example of a pinch analysis

The example in this section is taken from Kemp [49].

This example considers four stream, two hot and two cold, with a constant heat capacity are considered. A minimal temperature difference of 10 °C is imposed. Table B.5 shows the streams and their specifics. Besides the actual temperature of the streams, an interval temperature of each stream is defined. For hot stream this is the actual temperature minus half of the minimum temperature difference, for cold stream half of the minimum temperature difference is added to the actual temperature. This is done to define intervals in which stream are able to exchange heat with one another.

Next, the problem is split into intervals based on the interval temperatures of each stream. For each interval a net enthalpy change is determined. This is positive in the case that the heat supplied by cooling down the hot streams is greater than the heat required by the cold stream in that specific interval. Excess heat from higher temperature intervals can be transfered to lower temperature intervals. Adding this excess heat produces the fourth column in Table B.6. The interval from 140 to 85 °C still has a deficit of 20 kW, making the system infeasible. In order to make the system feasible, a hot utility of 20 kW must be added to the system, column 5. This produces a surplus of energy in every interval except one, which is where the pinch is, 85 °C in this case. The surplus in the lowest interval represents cooling that must be supplied by an external source.

The resulting pinch diagram of the system, Fig. B.1, illustrates the changing heat capacities at the interval temperatures and the pinch temperature, where the imposed minimal temperature difference of 10 °C applies. The cold and hot utility are the horizontal difference between the hot and cold temperature-enthalpy curves.

The system can now split in two, one subsystem above the pinch and one below, Fig. B.2. From this picture the hot need for a hot and cold utility can be confirmed as well. A pinch analysis does not lead to a design of a heat exchanger network. It does however provide a very useful starting point for a design. It minimizes the need for hot and cold utilities, thus maximizing thermodynamic efficiency. The choice of the minimal temperature difference is a trade off between thermodynamic efficiency and size of the heat exchangers/cost.

Contrary to this example, the problems analyzed in this work differ on a few points. Firstly, the streams do not have constant heat capacities. As a consequence, the pinch temperature does not always coincide with an interval where a flow is begins or ends as is the case for constant heat capacities. Therefore, the problem should be evaluated at a more regular temperature interval than only the shifted in- and outlet temperature of each stream.

Secondly, the mass flow through the sCO_2 Brayton is an unknown variable in the problem that is to be solved by the pinch analysis. The same principles apply, but the analysis must be done in a different order of steps.

Finally, in order to solve the problem with this unknown variable, an additional constraint must be imposed. No external heat utility is possible.

Appendix C. Additional data for model validation

See Tables C.7–C.11.

Appendix D. Additional data for case studies

See Figs. D.3–D.7.

Appendix E. Acronyms

SOFC Solid Oxide Fuel Cell

MSR Methane Steam Reforming

WGS Water-Gas Shift

sCO_2 Supercritical Carbon Dioxide

IIR Indirect Internal Reforming

DIR Direct Internal Reforming

PCHE Printed Circuit Heat Exchanger

ASR Area Specific Resistance

LHV Lower Heating Value

HHV Higher Heating Value

MCFC Molten Carbonate Fuel Cell

LMTD Logarithmic Mean Temperature Difference

GT Gas Turbine

CHP Combined Heat and Power

CSP Concentrated Solar Power

TIT Turbine Inlet Temperature

HRSG Heat Recovery Steam Generator

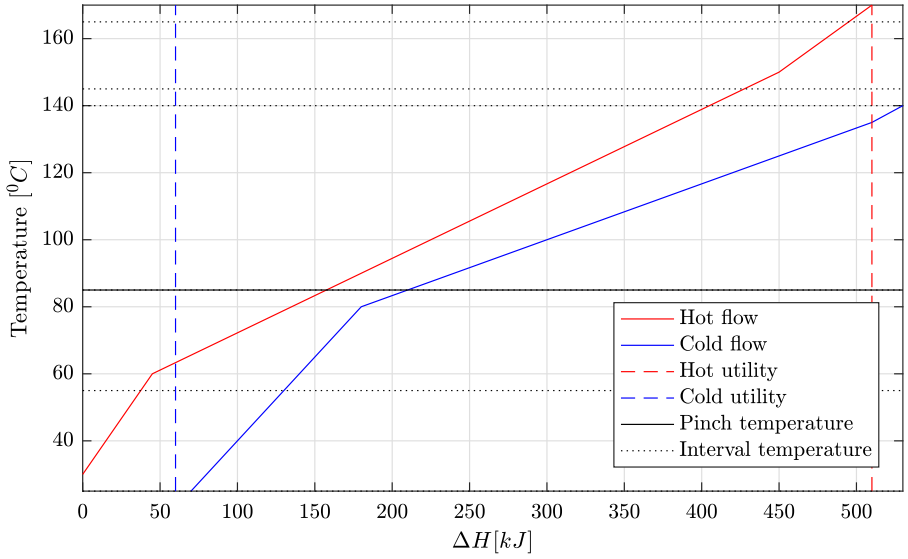

Fig. B.1. Pinch diagram (pinch analysis example).

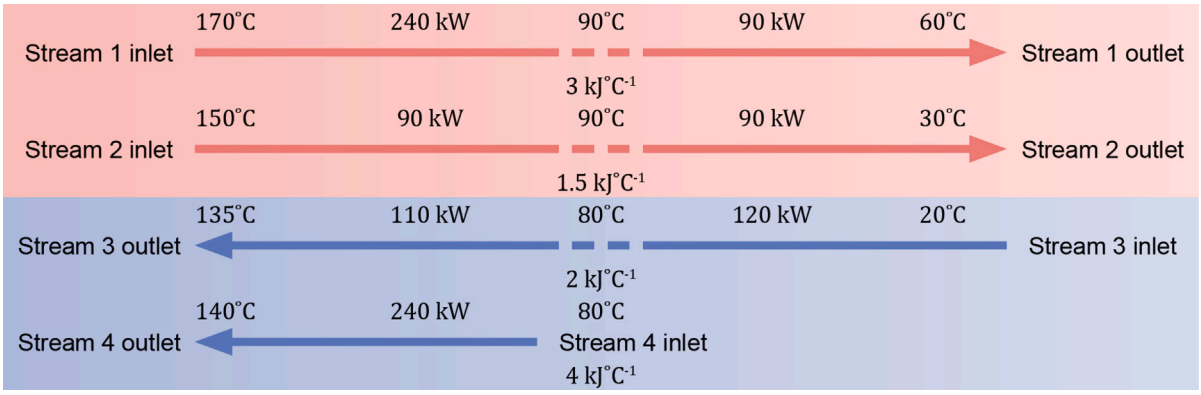

Fig. B.2. Heat flows (pinch analysis example).

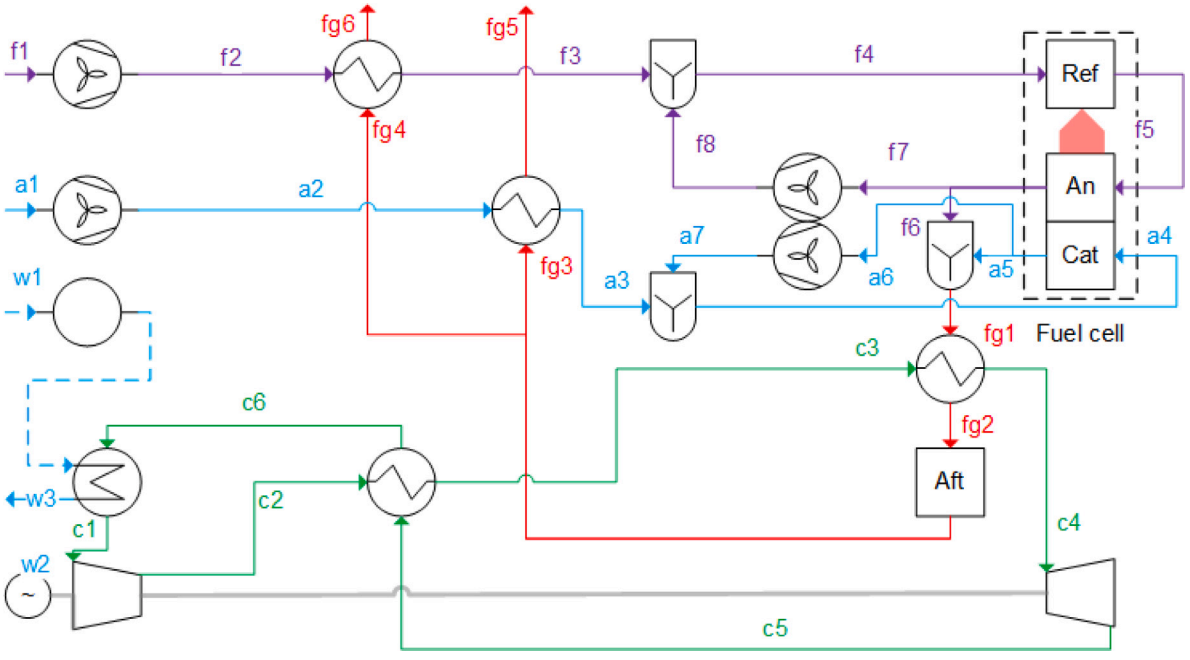

Fig. D.3. PFD (Case II: Cathode recirculation).

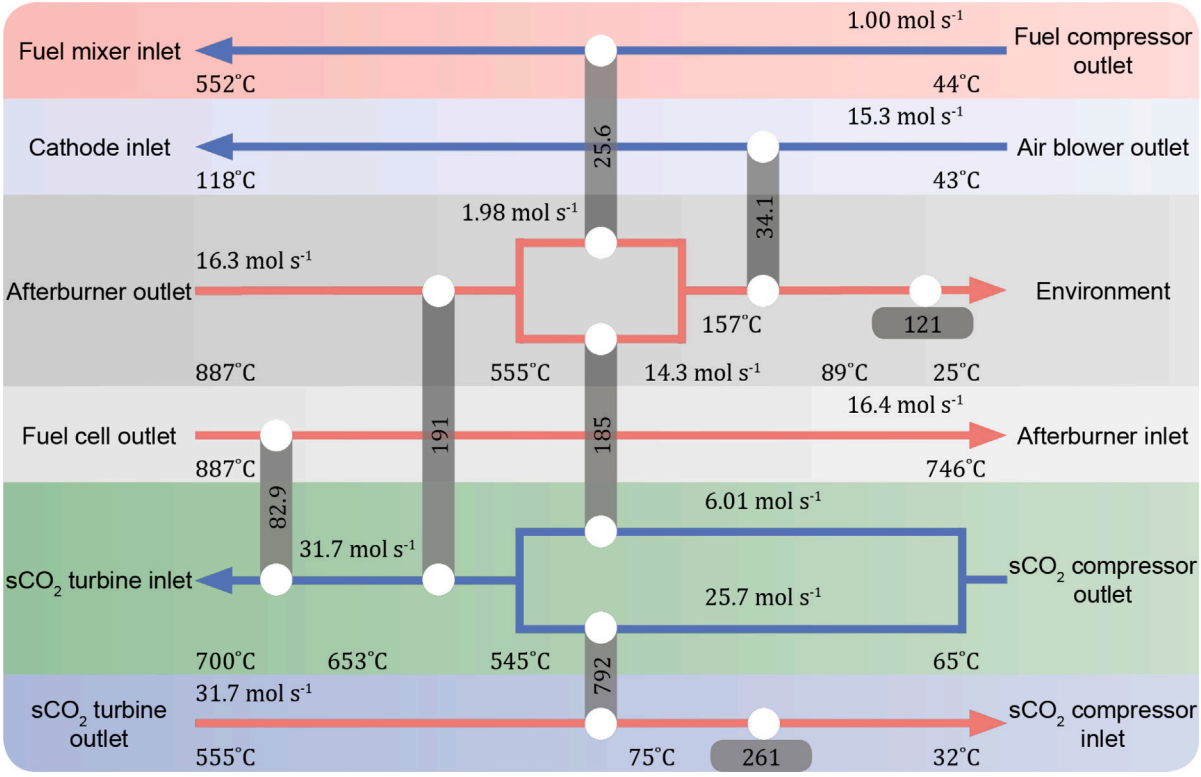

Fig. D.4. Heat exchanger network (case III.D: Cathode recirculation ratio, ΔT_{hex} = 10 °C, r_{ca} = 86%).

ER External Reforming

ORC Organic Rankine Cycle

PR Pressure Ratio

BoP Balance of Plant

DC Direct Current

AC Alternating Current

LP Low Pressure

HP High Pressure

TOT Turbine Outlet Temperature

STHE Shell and Tube Heat Exchanger

ST Steam Turbine

LTC Low temperature compressor

HTC High Temperature Compressor

LTR Low Temperature Recuperator

HTR High Temperature Recuperator

PFD Process Flow Diagram

HT High Temperature

LT Low Temperature

Table B.5
Stream data (pinch analysis example).

Stream	CP(kW/°Celsius)	Actual temperature (°C)		Interval temperature (°C)	
		Inlet	Outlet	Inlet	Outlet
1 (hot)	3	170	60	165	55
2 (hot)	1.5	150	30	145	25
3 (cold)	2	20	135	25	140
4 (cold)	4	80	140	85	145

Table B.6
Interval data (pinch analysis example).

Interval temperature (°C)	Streams	ΔH^{int} (kW)	$\Sigma\Delta H^{int}$ (kJ)	Shifted $\Sigma\Delta H^{int}$ (kJ)
165				+20
145	1	+60	+60	+80
140	1+2–4	+2.5	+62.5	+82.5
85	1+2-3–4	−82.5	−20	0
55	1+2–3	+75	+55	+75
25	2–3	−15	+40	+60

Table C.7
Comparison with Campanari and Iora [29].

Input (T_{FC}(°C)/i(A m^{-2}))	Output (Ohmic overpotential (mV))		
	Campanari and Iora	This study	Difference (%)
706/1635	169	164.5	−2.48
754/2135	178	173.7	−2.54
836/2321	161	152.8	−4.92
891/2099	132	127.7	−3.06
939/1481	89	86.1	−3.70
Input	Output		
	Campanari and Iora	This study	Difference (%)
Operating pressure, anode- inlet flow composition and outlet temperature and fuel utilization ratio	$x_{an,L}^{CH_4} = 0.00$	0.00	0.00
	$x_{an,L}^{H_2O} = 0.5128$	0.5075	−1.04
	$x_{an,L}^{CO} = 0.0853$	0.0772	−9.48
	$x_{an,L}^{CO_2} = 0.2420$	0.2466	+1.88
	$x_{an,L}^{H_2} = 0.1143$	0.1171	+2.45
	$I = 1.72 \times 10^5$ A	1.72×10^5 A	0.00
Input (T_{FC}(°C)/i(A cm^{-2})[a]	Output (Power density (mW cm^{-2}))		
	Campanari and Iora	This study	Difference (%)
796.5/179.2	123.6	133.23	+7.77
739/179.2	123.6	132.54	+7.22
835/179.2	123.6	132.37	+7.08

[a]Concentration of hydrogen, water and oxygen as well as total current is as calculated in present work

Table C.8
Comparison with Asimptote [44].

Input	Output		
	Asimptote	This study	Difference (%)
Reformer inlet conditions, fuel cell and reformer operating pressures and temperatures, fuel utilization ratio, ohmic resistance and current density	$x_{an,L}^{CH_4} = 0.0018$	0.0019	+5.56
	$x_{an,L}^{H_2O} = 0.6005$	0.6005	0.00
	$x_{an,L}^{CO} = 0.0387$	0.0385	−0.52
	$x_{an,L}^{CO_2} = 0.2940$	0.2942	+0.07
	$x_{an,L}^{H_2} = 0.0650$	0.0649	−0.15
	$\dot{W}_{FC,e} = 442.86$ kW	400.11	−9.65

Table C.9
Comparison with Chan et al. [11].

Input	Output		
	Chan et al.	This study	Difference (%)
Operating pressure, anode inlet flow composition, anode outlet and stack temperature, fuel utilization ratio and number of cells	$x_{an,L}^{CH_4} = 0.0006$	0	–
	$x_{an,L}^{H_2O} = 0.6175$	0.6553	+4.42
	$x_{an,L}^{CO} = 0.0499$	0.0414	−17.8
	$x_{an,L}^{CO_2} = 0.1619$	0.1733	+7.02
	$x_{an,L}^{H_2} = 0.1569$	0.1268	−19.17
	$i = 141.6$ A m^{-2}	154.3 A m^{-2}	+8.94
	$E_{FC} = 0.738$ V	0.7367 V	−3.56
	$\eta_{FC} = 52.19\%$	54.83%	+5.06%

Table C.10
Comparison with Aguiar et al. [45].

Input	Output		
	Aguiar et al.	This study	Difference (%)
Operating pressure, reformer inlet composition, reformer and anode outlet temperature, cell operating voltage and current density	$x_{rf,L}^{CH_4} = 0.00$	0.00	0.00
	$x_{rf,L}^{CO} = 0.25$	0.32	+28.4
	$x_{rf,L}^{H_2} = 0.45$	0.37	−17.01
	$x_{an,L}^{CH_4} = 0.00$	0.00	0.00
	$x_{an,L}^{CO} = 0.12$	0.09	−26.00
	$x_{an,L}^{H_2} = 0.15$	0.13	−14.27
	$\eta_{FC} = 46.5\%$	46.45%	−0.1

Table C.11
Comparison with Aguiar et al. [46].

Input	Output		
	Aguiar et al.	This study	Difference (%)
Operating pressure, anode inlet composition, anode outlet temperature, cell operating voltage and current density	$x_{an,L}^{CH_4} = 0.00$	0.00	0.00
	$x_{an,L}^{H_2O} = 0.65$	0.63	−2.36
	$x_{an,L}^{CO} = 0.04$	0.035	−13.42
	$x_{an,L}^{CO_2} = 0.16$	0.17	+3.35
	$x_{an,L}^{H_2} = 0.15$	0.17	+10.24
	$\eta_{FC} = 46.8\%$	47.8%	+2.18

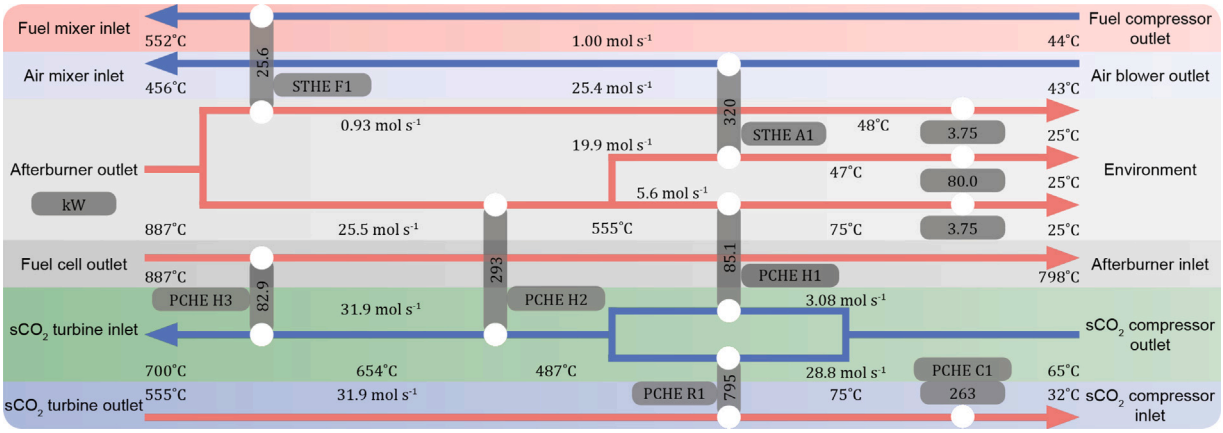

Fig. D.5. Heat exchanger network (case III: Cathode recirculation ratio, $\Delta T_{hex} = 10\,°C$, $r_{ca} = 74.86\%$).

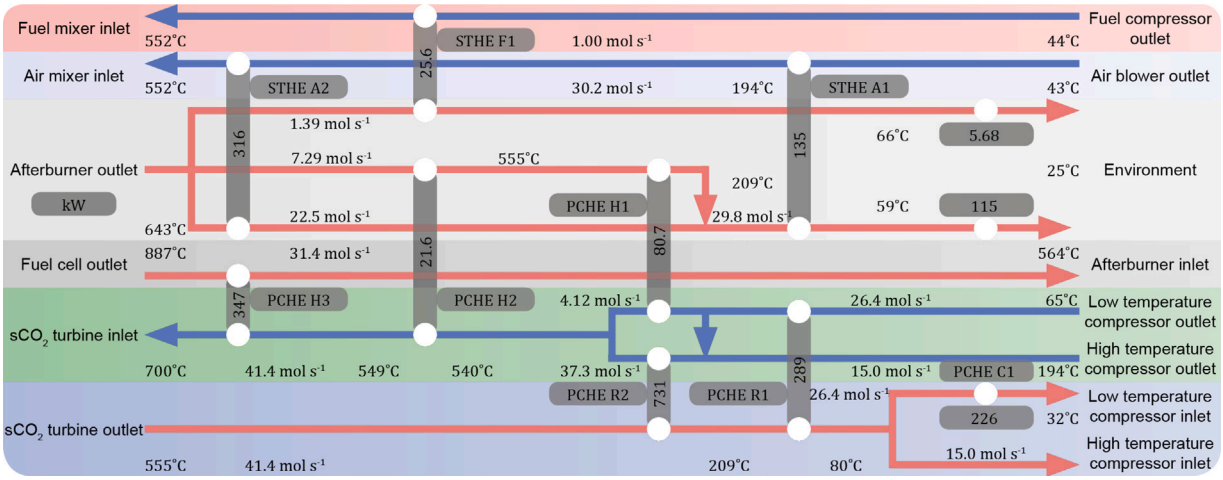

Fig. D.6. Heat exchanger network (Case IV, $\Delta T_{hex} = 15\,°C$).

SSHS solid oxide fuel cell- supercritical carbon dioxide Brayton cycle hybrid system

hex Heat Exchanger

Appendix F. Nomenclature

A	area
CP	isobaric heat capacity
C_P	specific isobaric heat capacity
δ	electron path length
ΔH^0	enthalpy of formation
ΔG^0	Gibbs free energy of formation
η	efficiency
E	potential
F	Faraday constant
i	current density
I	current
K	chemical equilibrium constant
$I, II, III, ...$	rank in temperature from low to high
L	flow length
$\dot{m}$	molar flow rate
N	number of
P	pressure

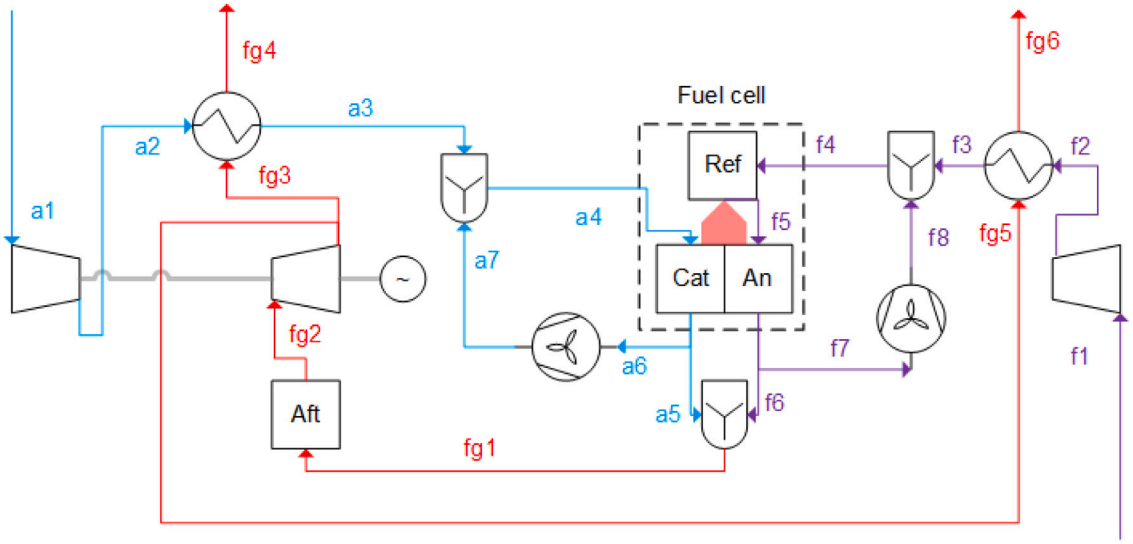

Fig. D.7. PFD (Case V).

$\dot{Q}$	heat
$\bar{R}$	universal gas constant
R	ohmic resistance
ρ	resistivity
r	recirculation ratio
S/C	steam to carbon ratio
T	temperature
$\bar{U}$	overall heat transfer coefficient
$\dot{W}$	work
U_f	fuel utilization ratio
V	volume
x	concentration
ξ	extent of reaction
0	environment
aft	afterburner
an	anode
ic	interconnection
e	electric
E	entering stream
FC	fuel cell
fd	feed
pre	preheater
hex	heat exchanger
rf	reformer
C	cold stream
com	compressor
H	hot stream
h	specific isobaric heat capacity
ca	cathode
tur	turbine
N	Nernst
gen	generator
$flue$	flue gas
k	component k
com	compressor
int	interval
Ω	ohmic

References

[1] Larminie James, Dicks Andrew. Fuel cell systems explained. 2nd ed. Chichester, West Sussex: J. Wiley; 2003, Knovel URL http://www.knovel.com/knovel2/Toc.jsp?BookID=1109.

[2] Dostal V, Driscoll MJ, Hejzlar P. A supercritical crabon dioxide cycle for next generation nuclear reactors (Thesis), Massachusetts Institute of Technology; 2004, URL http://web.mit.edu/22.33/www/dostal.pdf.

[3] Ahn Yoonhan, Bae Seong Jun, Kim Minseok, Cho Seong Kuk, Baik Seungjoon, Lee Jeong Ik, et al. Review of supercritical CO_2 power cycle technology and current status of research and development. Nucl Eng Technol 2015;47(6):647–61. http://dx.doi.org/10.1016/j.net.2015.06.009, URL http://www.sciencedirect.com/science/article/pii/S1738573315001606.

[4] Song Jian, song Li Xue, dong Ren Xiao, wei Gu Chun. Performance improvement of a preheating supercritical CO_2 (S-CO_2) cycle based system for engine waste heat recovery. Energy Convers Manage 2018;161:225–33. http://dx.doi.org/10.1016/j.enconman.2018.02.009, URL http://www.sciencedirect.com/science/article/pii/S0196890418301055.

[5] Schifflechner Christopher, Dawo Fabian, Eyerer Sebastian, Wieland Christoph, Spliethoff Hartmut. Combined heat and power generation by enhanced geothermal systems: Comparison of direct and indirect concepts for water and supercritical CO_2 as heat carriers. In: 5th international seminar on ORC power systems, Athens, Greece, 2019.

[6] Al-Sulaiman Fahad A, Atif Maimoon. Performance comparison of different supercritical carbon dioxide brayton cycles integrated with a solar power tower. Energy 2015;82:61–71. http://dx.doi.org/10.1016/j.energy.2014.12.070, URL http://www.sciencedirect.com/science/article/pii/S0360544214014509.

[7] Turchi Craig. 10 MW supercritical CO_2 turbine test. Report DE-EE0002589 United States 10.2172/1117025 NREL English, Golden, CO (United States): National Renewable Energy Laboratory (NREL); 2014, URL http://www.osti.gov/scitech/servlets/purl/1117025.

[8] Eguchi K, Singhal SC, editors. ECS transaction, vol. 91. 2019, URL http://ecst.ecsdl.org/content/91/1.

[9] Buonomano Annamaria, Calise Francesco, d'Accadia Massimo Dentice, Palombo Adolfo, Vicidomini Maria. Hybrid solid oxide fuel cells–gas turbine systems for combined heat and power: A review. Appl Energy 2015;156:32–85. http://dx.doi.org/10.1016/j.apenergy.2015.06.027, URL http://www.sciencedirect.com/science/article/pii/S0306261915007850.

[10] Calise F, Dentice d' Accadia M, Vanoli L, von Spakovsky Michael R. Full load synthesis/design optimization of a hybrid SOFC–GT power plant. Energy 2007;32(4):446–58. http://dx.doi.org/10.1016/j.energy.2006.06.016, URL http://www.sciencedirect.com/science/article/pii/S036054420600171X.

[11] Chan SH, Ho HK, Tian Y. Modelling of simple hybrid solid oxide fuel cell and gas turbine power plant. J Power Sources 2002;109(1):111–20. http://dx.doi.org/10.1016/S0378-7753(02)00051-4, URL http://www.sciencedirect.com/science/article/pii/S0378775302000514.

[12] Chan SH, Ho HK, Tian Y. Multi-level modeling of SOFC–gas turbine hybrid system. Int J Hydrogen Energy 2003;28(8):889–900. http://dx.doi.org/10.1016/S0360-3199(02)00160-X, URL http://www.sciencedirect.com/science/article/pii/S036031990200160X.

[13] Song Tae Won, Sohn Jeong Lak, Kim Jae Hwan, Kim Tong Seop, Ro Sung Tack, Suzuki Kenjiro. Performance analysis of a tubular solid oxide fuel cell/micro gas turbine hybrid power system based on a quasi-two dimensional model. J Power Sources 2005;142(1–2):30–42. http://dx.doi.org/10.1016/j.jpowsour.2004.10.011, URL http://www.sciencedirect.com/science/article/pii/S0378775304010845.

[14] Jia Junxi, Abudula Abuliti, Wei Liming, Shi Yue. Performance comparison of three solid oxide fuel cell power systems. Int J Energy Res 2013;37(14):1821–30. http://dx.doi.org/10.1002/er.3000, URL http://dx.doi.org/10.1002/er.3000.

[15] Yang WJ, Park SK, Kim TS, Kim JH, Sohn JL, Ro ST. Design performance analysis of pressurized solid oxide fuel cell/gas turbine hybrid systems considering temperature constraints. J Power Sources 2006;160(1):462–73. http://dx.doi.org/10.1016/j.jpowsour.2006.01.018, URL http://www.sciencedirect.com/science/article/pii/S0378775306000887.

[16] Arsalis Alexandros. Thermoeconomic modeling and parametric study of hybrid SOFC–gas turbine–steam turbine power plants ranging from 1.5 to 10 MWe. J Power Sources 2008;181(2):313–26. http://dx.doi.org/10.1016/j.jpowsour.2007.11.104, URL http://www.sciencedirect.com/science/article/pii/S0378775307026407.

[17] Park SK, Kim TS. Comparison between pressurized design and ambient pressure design of hybrid solid oxide fuel cell–gas turbine systems. J Power Sources 2006;163(1):490–9. http://dx.doi.org/10.1016/j.jpowsour.2006.09.036, URL http://www.sciencedirect.com/science/article/pii/S0378775306019410.

[18] Facchinetti E, Favrat D, Marechal F. Design and optimization of an innovative solid oxide fuel cell–gas turbine hybrid cycle for small scale distributed generation. Fuel Cells 2014;14(4):595–606. http://dx.doi.org/10.1002/fuce.201300196, URL http://dx.doi.org/10.1002/fuce.201300196.

[19] Bae Seong Jun, Ahn Yoonhan, Lee Jekyoung, Lee Jeong Ik. Various supercritical carbon dioxide cycle layouts study for molten carbonate fuel cell application. J Power Sources 2014;270:608–18. http://dx.doi.org/10.1016/j.jpowsour.2014.07.121, URL http://www.sciencedirect.com/science/article/pii/S0378775314011756.

[20] Lemmon EW, Huber ML, McLinden MO. NIST Standard reference database 23, Version 9.0. 2010, URL http://webbook.nist.gov/chemistry/.

[21] Chase MW. National institute of, standards and technology NIST-JANAF thermochemical tables. Washington, D.C., Woodbury, N.Y.: American Chemical Society, American Institute of Physics for the National Institute of Standards and Technology; 1998, (U.S.).

[22] Ahmed Khaliq, Föger Karl. Fuel processing for high-temperature high-efficiency fuel cells. Ind Eng Chem Res 2010;49(16):7239–56. http://dx.doi.org/10.1021/ie100778g, URL http://dx.doi.org/10.1021/ie100778g.

[23] Sui S, Xiu GH. Fuels and fuel processing. In: High-temperature solid oxide fuel cells for the 21st century. 2nd ed. Boston: Academic Press; 2016, p. 461–95. http://dx.doi.org/10.1016/B978-0-12-410453-2.00014-2, URL http://www.sciencedirect.com/science/article/pii/B9780124104532000142.

[24] Bossel Ulf, Dubal Léo. Facts & figures : final report on SOFC data. Berne: Swiss Federal Office of Energy, Operating Agent Task II; 1992.

[25] Aravind PV, Woudstra T, Woudstra N, Spliethoff H. Thermodynamic evaluation of small-scale systems with biomass gasifiers, solid oxide fuel cells with Ni/GDC anodes and gas turbines. J Power Sources 2009;190(2):461–75. http://dx.doi.org/10.1016/j.jpowsour.2009.01.017, URL http://www.sciencedirect.com/science/article/pii/S0378775309000561.

[26] Holyst Robert, Poniewierski Andrzej. Thermodynamics for chemists, physicists and engineers. Springer; 2012, URL http://dx.doi.org/10.1007/978-94-007-2999-5.

[27] EG& G Technical Services, Inc. Fuel cell handbook. 7th ed. BusinessTechnology Books; 2004.

[28] Minh NQ. Cell and stack design, fabrication and performance. In: High-temperature solid oxide fuel cells for the 21st century. 2nd ed. Boston: Academic Press; 2016, p. 255–82. http://dx.doi.org/10.1016/B978-0-12-410453-2.00008-7, URL http://www.sciencedirect.com/science/article/pii/B9780124104532000087.

[29] Campanari S, Iora P. Definition and sensitivity analysis of a finite volume SOFC model for a tubular cell geometry. J Power Sources 2004;132(1–2):113–26. http://dx.doi.org/10.1016/j.jpowsour.2004.01.043, URL http://www.sciencedirect.com/science/article/pii/S0378775304001454.

[30] Bessette II Norman F, Wepfer William J, Winnick Jack. A mathematical model of a solid oxide fuel cell. J Electrochem Soc 1995;142:3792–800. http://dx.doi.org/10.1149/1.2048415, URL http://jes.ecsdl.org/content/142/11/3792.short.

[31] Omosun AO, Bauen A, Brandon NP, Adjiman CS, Hart D. Modelling system efficiencies and costs of two biomass-fuelled SOFC systems. J Power Sources 2004;131(1–2):96–106. http://dx.doi.org/10.1016/j.jpowsour.2004.01.004, URL http://www.sciencedirect.com/science/article/pii/S0378775304000266.

[32] Bahamonde Noriega JS, Colonna P, Boersma BJ. Design method for s-CO_2 gas turbine power plants: Integration of thermodynamic analysis and components design for advanced applications (Thesis), Delft University of Technology; 2012, Item Resolution URL http://resolver.tudelft.nl/uuid:e157e264-f384-4641-8293-8362fb0dc7f9.

[33] Neises T, Turchi C. A comparison of supercritical carbon dioxide power cycle configurations with an emphasis on CSP applications. Energy Procedia 2014;49:1187–96. http://dx.doi.org/10.1016/j.egypro.2014.03.128, URL http://www.sciencedirect.com/science/article/pii/S1876610214005827.

[34] Kulhanek Martin, Dostal Vaclav. Supercritical carbon dioxide cycles thermodynamic analysis and comparison. In: Supercritical CO_2 power cycle symposium, Boulder, CO, May, 2011, pp. 24–25.

[35] Bidkar Rahul A, Mann Andrew, Singh Rajkeshar, Sevincer Deip, Cich Stefan, Day Meera, Kulhanek Chris D, Thatte Azam M, Peter Andrew M, Hofer Doug, Moore Jeff. Conceptual designs of $50MW_e$ and $450MW_e$ supercritical CO_2 turbomachinery trains for power generation from coal. Part 1: Cycle and turbine. 2016, URL http://www.swri.org/4org/d18/sCO2/papers2016/Turbomachinery/071pt1paper.pdf.

[36] Bidkar Rahul A, Musgrove Grant, Day Meera, Kulhanek Chris D, Allison Tim, Peter Andrew M, Hofer Doug, Moore Jeff. Conceptual designs of $50MW_e$ and $450MW_e$ supercritical CO_2 turbomachinery trains for power generation from coal. Part 2: Compressors. 2016, URL http://www.swri.org/4org/d18/sCO2/papers2016/Turbomachinery/072pt2paper.pdf.

[37] Haseli Y, Dincer I, Naterer GF. Thermodynamic modeling of a gas turbine cycle combined with a solid oxide fuel cell. Int J Hydrogen Energy 2008;33(20):5811–22. http://dx.doi.org/10.1016/j.ijhydene.2008.05.036, URL http://www.sciencedirect.com/science/article/pii/S036031990800548X.

[38] Towler Gavin, Sinnott Ray K. Chemical engineering design - principles, practice and economics of plant and process design. Elsevier; 2013, URL http://app.knovel.com/hotlink/toc/id:kpCEDPPEP4/chemical-engineering/chemical-engineering.

[39] Heatric. Typical characteristics of diffusion-bonded heat exchangers, vol. 2017, no. 20/02. 2017, URL http://www.heatric.com/typical_characteristics_of_PCHEs.html.

[40] Hesselgreaves John E, Law Richard, Reay David A. Compact heat exchangers - selection, design and operation. 2nd ed. Elsevier; 2017, URL http://app.knovel.com/hotlink/pdf/id:kt0119EPI3/compact-heat-exchangers/straight-channels.

[41] Mills Anthony F. Heat transfer. 2nd ed. Upper Saddle River, N.J.: Prentice Hall; 1999.

[42] Oyakawa Kenyu, Shinzato Takao, Mabuchi Ikuo. The effects of the channel width on heat-transfer augmentation in a sinusoidal wave channel. JSME Int J II 1989;32(3):403–10, URL http://ci.nii.ac.jp/naid/110002494279/en/.

[43] Song Hoseok. Investigation of a printed circuit heat exchanger for supercritical CO_2 and water (Thesis), Kansas State University; 2007, URL https://krex.k-state.edu/dspace/bitstream/handle/2097/346/HoseokSong2007.pdf?sequence=1.

[44] Asimptote. Cycle-Tempo. 2011, URL http://www.asimptote.nl/software/cycle-tempo/.

[45] Aguiar P, Chadwick D, Kershenbaum L. Modelling of an indirect internal reforming solid oxide fuel cell. Chem Eng Sci 2002;57(10):1665–77. http://dx.doi.org/10.1016/S0009-2509(02)00058-1, URL http://www.sciencedirect.com/science/article/pii/S0009250902000581.

[46] Aguiar P, Adjiman CS, Brandon NP. Anode-supported intermediate temperature direct internal reforming solid oxide fuel cell. I: model-based steady-state performance. J Power Sources 2004;138(1–2):120–36. http://dx.doi.org/10.1016/j.jpowsour.2004.06.040, URL http://www.sciencedirect.com/science/article/pii/S0378775304006950.

[47] Singhal SC. Advances in solid oxide fuel cell technology. Solid State Ion 2000;135(1–4):305–13. http://dx.doi.org/10.1016/S0167-2738(00)00452-5, URL http://www.sciencedirect.com/science/article/pii/S0167273800004525.

[48] Schöffer Samuel Ivo, Klein Sikke, Aravind Purushothaman Vellayani, Pecnik Rene, Infante Ferreira Carlos. A solid oxide fuel cell- sCO_2 brayton cycle hybrid system. 2017, URL http://resolver.tudelft.nl/uuid:f7992e05-970e-47b0-ae05-05dd0ad0bad1.

[49] Kemp Ian C. Pinch analysis and process integration : a user guide on process integration for the efficient use of energy. 2nd ed. Oxford: Butterworth-Heinemann; 2007.